optica

Cavity quantum electrodynamics with color centers in diamond

ERIKA JANITZ,[1,†] MIHIR K. BHASKAR,[2,†] AND LILIAN CHILDRESS[1,*]

[1]Department of Physics, McGill University, 3600 Rue University, Montréal, Québec H3A 2T8, Canada
[2]Department of Physics, Harvard University, 17 Oxford St., Cambridge, Massachusetts 02138, USA
*Corresponding author: lilian.childress@mcgill.ca

Received 26 May 2020; revised 27 July 2020; accepted 4 August 2020 (Doc. ID 398628); published 21 September 2020

Coherent interfaces between optical photons and long-lived matter qubits form a key resource for a broad range of quantum technologies. Cavity quantum electrodynamics (cQED) offers a route to achieve such an interface by enhancing interactions between cavity-confined photons and individual emitters. Over the last two decades, a promising new class of emitters based on defect centers in diamond has emerged, combining long spin coherence times with atom-like optical transitions. More recently, advances in optical resonator technologies have made it feasible to realize cQED in diamond. This article reviews progress towards coupling color centers in diamond to optical resonators, focusing on approaches compatible with quantum networks. We consider the challenges for cQED with solid-state emitters and introduce the relevant properties of diamond defect centers before examining two qualitatively different resonator designs: micrometer-scale Fabry–Perot cavities and diamond nanophotonic cavities. For each approach, we examine the underlying theory and fabrication, discuss strengths and outstanding challenges, and highlight state-of-the-art experiments.

https://doi.org/10.1364/OPTICA.398628

1. INTRODUCTION

The last two decades have seen an explosive growth in quantum technologies, with remarkable advances in cryptography [1–4], computing [5], and metrology [6]. Motivated by the success of the classical internet and the promise of quantum-secured communication, considerable interest has arisen in developing so-called quantum networks [7,8]. Such networks comprise nodes capable of storing and processing quantum information, connected by quantum-coherent photonic channels, and could enable distributed quantum computing [9–11], quantum-enhanced clock synchronization [12–14] and interferometry [15,16], as well as long-distance quantum communication [17–19].

Optical photons play a critical role in quantum networks because they interact very weakly with surrounding media, making them the ideal carrier of quantum information over long distances. However, these weak interactions pose a significant impediment for engineering gates between photons, and make it difficult to interface photons with information storage and processing nodes. Cavity quantum electrodynamics (cQED) offers a paradigm to overcome these challenges: by confining photons inside a high quality factor optical resonator, vastly enhanced interactions with material systems can be obtained [20–25], enabling a broad range of relevant quantum information tasks [26–28]. For example, cavity-coupled emitters can be used as bright sources of the indistinguishable photons [29,30] needed for photonic quantum computation [31,32], or even employed to mediate interactions between photons [33]. The most exciting opportunities emerge when the material system possesses long-lived internal degrees of freedom, such as electron or nuclear spin sublevels, in addition to its optical transitions [an example is shown in Fig. 1(b)]. Such long-lived states can be used to realize a quantum memory for light [34–37], spin–photon entanglement [38–43], spin–photon switches [44,45], or quantum gates between asynchronous photons [46–48]. While some of these capabilities can be realized without cavities (e.g., using optically dense ensembles [49,50]), cQED can enhance the efficiency of probabilistic protocols, and even enable near-deterministic interactions between single photons and individual quantum bits.

The likely impact of cQED systems on quantum networks is exemplified by their potential role in quantum repeaters, which compensate for photon loss to enable transmission of quantum states or secret keys over long distances [17–19]. The simplest repeater schemes distribute entanglement via a chain of spins linked by photonic channels [17], generating a resource that can be purified [51–53] and used to teleport quantum information [54,55] or generate a secret key [56]. Such schemes often employ heralded entanglement generation [57–64], which exploits entanglement between spins and indistinguishable outgoing photons, such that a detected photon could have originated from either of two distant spins. Conditioned on one ore more detection event(s), the spins are projected onto an entangled state, and photon loss errors result only in reduced success probability. Cavity coupling can vastly increase the efficiency of these protocols by increasing photon emission rates into a well-defined cavity-coupled mode [20,65]; for strongly coupled cQED systems, even deterministic remote entanglement generation can be possible [27,66]. In

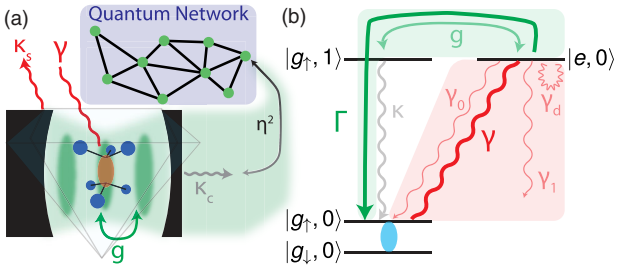

Fig. 1. (a) Schematic of diamond cQED system. Cavity photons are coherently coupled to the color center at rate g and can scatter out of the cavity at rate κ_s, or into a collected mode at rate κ_c. Optical decoherence of the color center occurs at rate γ. Indistinguishable photons in the collected mode are matched into a single-mode fiber with efficiency η^2. (b) Detailed diagram for one instance of relevant cQED energy levels, comparing coherent coupling rates (green) to decoherence rates (gray, red). Quantum information (blue oval) is stored in the color center spin states $|g_\downarrow, 0\rangle$, $|g_\uparrow, 0\rangle$, where $g(e)$ indicates the ground (excited) state, $\uparrow, \downarrow$ indicate spin, and the final integer indicates cavity photon number. $|e, 0\rangle$ couples spin-selectively to $|g_\uparrow, 1\rangle$ at rate g, leading to an effective cavity-enhanced emission rate Γ. The cavity dissipates at overall decay rate $\kappa = \kappa_s + \kappa_c$, and the emitter dephases at overall rate γ, which comprises desired emission (γ_0), undesired decay (γ_1), and pure dephasing (γ_d).

the longer term, one-way repeater schemes promise much faster communication by transmitting entangled multi-photon states that encode quantum information in a photon-loss-tolerant structure [67,68], potentially incorporating error correction [69], and without the need for long-term quantum memory [70–72]. In this context, cavity-coupled emitters play an essential role: by maintaining a coherent quantum memory during repeated interactions with light, an emitter can generate entanglement between sequentially emitted photons [73–76] and be used for efficient re-encoding at one-way repeater stations [77]. While these are just a subset of quantum repeater and networking functionalities being actively pursued, they illustrate the key role played by cavity-coupled spin–photon interfaces in near-term quantum information applications [78].

A wide variety of physical platforms for realizing cQED are currently being explored, aimed at achieving interaction rates between the quantum emitter and cavity mode that exceed relevant losses. Cavity-enhanced interfaces between optical photons and individual quantum emitters began with neutral atoms [25] and quickly expanded to other systems including quantum dots [79], molecules [80], and trapped ions [81,82]. In particular, there has been a recent interest in cavity coupling to atom-like solid-state systems [83,84], most notably defects in diamond [85–87], but also rare-earth ions [88,89], defects in silicon carbide [90], and potentially others [91]. These defect-based systems aim to combine the atom-like advantages of a predictable structure, optical selection rules, and long spin coherence times with a robust solid-state platform compatible with integration into micro- or nano-scale cavities. The various host materials and defect structures carry different strengths, as discussed in recent reviews [83,84]. Here, we focus on the most well-studied platform for defect-based, optically active spin qubits: diamond.

Indeed, diamond's large bandgap and nearly nuclear-spin-free lattice make it an appealing host for such defects [92]. Of these, the best known is the nitrogen-vacancy (NV) center, which exhibits long spin coherence times, access to nearby nuclear spins for ancilla qubits [93], and well-understood spin-selective optical transitions [94,95]. Due to these properties, cavity-coupled NVs form the basis for many quantum information proposals [10,96–98]. Moreover, even without cavity coupling, NVs have already been used to achieve landmark proof-of-principle quantum network experiments demonstrating loophole-free Bell inequality violation [99], unconditional teleportation [100], entanglement distillation [53], and entanglement distribution faster than entanglement loss [101], all of which would exhibit vastly improved efficiency using cavity coupling. At the same time, novel defects such as the silicon vacancy (SiV) have been found to exhibit superior optical properties [87] and the potential for long spin coherence times [102–104]. These advances have helped to motivate development of cQED systems in diamond.

This paper reviews recent progress in coupling individual diamond defects to optical resonators, focusing on cQED platforms with a clear potential for quantum applications. Over the last decade, diamond defects have been coupled to a wide range of photonic and plasmonic systems, and we refer the reader to excellent reviews [85,86,105] for an overview. Here, we focus on two approaches with the strongest near-term promise for quantum networking applications. One avenue employs external Fabry–Perot microcavities [106,107] surrounding the defect center. While early work with defects in nanodiamond laid crucial groundwork [108–112], the chief advantage of Fabry–Perot microcavities for quantum networking applications is that they can enclose relatively thick (∼μm) diamond membranes [113] where defect centers are far from charge noise at surfaces [114]. This opens the possibility to work with highly sensitive NV centers and create a cQED platform that leverages nearly two decades of advances in NV quantum science. The second approach we consider fabricates high quality factor optical resonators from diamond itself [115,116]. While hybrid platforms combining diamond with other nanofabricated materials hold great future promise for advanced functionality and scale-up [117–121], we focus on the recent achievements and near-term potential of all-diamond devices, which have the advantage of maximizing cavity mode overlap with defects, and have recently seen breakthroughs in fabrication techniques that have enabled major cQED milestones to be reached [122–124]. An essential element of this recent success has been the use of novel diamond defects that are largely insensitive to proximal surface noise [87]. For each of these two methodologies, we review the underlying theory and fabrication considerations, highlight state-of-the-art achievements, and discuss the outstanding challenges. Indeed, recent progress in these two approaches has put the diamond defect community on the precipice of realizing key steps toward quantum networking enabled by an efficient and coherent photonic interface.

2. CAVITY QED WITH SOLID-STATE EMITTERS

Cavity QED enhances the coherent coupling rate between a quantum emitter and cavity-confined photons, thereby improving the efficiency with which indistinguishable photons (within the same spatial, spectral, and temporal mode) can interact with individual color center quantum memories. This can approach a deterministic process when the emitter–photon interaction rate exceeds cavity losses and dephasing of the emitter optical transition. In this section, we examine the figures of merit for cQED with imperfect emitters, and consider different regimes for quantum applications.

In the absence of a cavity, emitter–photon interactions scale with the spontaneous emission rate γ_0 along the desired optical transition. In the case of color centers (see Section 3), this is typically a transition within the zero phonon line (ZPL), and the rate γ_0 is often weak compared to the overall rate of dephasing of the optical transition (γ). The total dephasing rate γ comprises both γ_0 and all other decay pathways (γ_1), including nonradiative decay or emission into the phonon sideband (PSB), as well as pure dephasing (γ_d), with $\gamma = \gamma_0 + \gamma_1 + \gamma_d$ [Fig. 1(b)].

When an emitter is placed inside of an optical cavity, the local photonic density of states can be strongly enhanced at the cavity resonance frequency, enabling rapid emitter–photon interactions when the cavity is tuned to the emitter optical transition. This enhancement can be characterized using the *Purcell factor*

$$\mathcal{P} = \frac{\Gamma}{\gamma_0}, \tag{1}$$

which compares Γ, the new rate of emission via the cavity, to γ_0, the original free-space emission rate along the relevant transition. Note that definitions of the Purcell factor vary, especially for non-ideal emitters, and we have chosen this definition to clearly differentiate the regimes of cQED with broadened emitters. When the emitter is on resonance with the cavity, and the cavity decay κ is the dominating rate, $\Gamma \approx 4g^2/\kappa$. Here, $g = \vec{\mu} \cdot \vec{\mathcal{E}}_0/\hbar$ is the rate of interaction between the dipole moment $\vec{\mu}$ of the optical transition of interest and the cavity mode vacuum field $\vec{\mathcal{E}}_0$ at the emitter location. Notably, since $\gamma_0 \propto \mu^2$, μ drops out of $\mathcal{P}$, and for an optimally oriented and located emitter, the Purcell factor is determined entirely by the properties of the cavity [65,125]:

$$\mathcal{P} = \frac{3}{4\pi^2}\left(\frac{\lambda}{n}\right)^3\left(\frac{Q}{V}\right), \tag{2}$$

where $Q = \omega/\kappa$ is the quality factor of the cavity, ω is its resonance frequency, λ is the corresponding wavelength in free space, n is the index of refraction within the cavity (assumed constant), and the cavity mode volume V emerges from $\mathcal{E}_0 \propto 1/\sqrt{V}$ [126]. The scaling of $\mathcal{P} \propto Q/V$ naturally motivates the use of high quality factor cavities with minimal mode volume.

$\mathcal{P}$ quantifies the enhancement of radiative emission on resonance with the cavity. However, for most solid-state emitters, the resonant optical emission γ_0 accounts for only a fraction of their total decay processes $\gamma_0 + \gamma_1$, implying that $\mathcal{P}$ does not describe the increase in the overall excited-state decay rate. Furthermore, $\mathcal{P}$ does not specify the absolute probability of coherent atom–photon interaction per attempt; this depends on the cooperativity C, where

$$C = \frac{4g^2}{\kappa\gamma} = \mathcal{P}\left(\frac{\gamma_0}{\gamma}\right) \equiv \frac{\Gamma}{\gamma}. \tag{3}$$

Here, the final equivalence (valid in the large-κ limit), gives a physical picture of C: the cooperativity compares the rate of radiation via the cavity to all emitter dephasing mechanisms. More generally, when $C > 1$, the coherent coupling between the emitter and cavity photons is stronger than the decoherence mechanisms, leading to near-deterministic atom–photon interactions [25,78].

Unlike the Purcell factor $\mathcal{P}$, the cooperativity C captures the effects of the sub-optimal optical characteristics of solid-state emitters. In the case of an ideal, radiatively broadened two-level system, $\gamma_0/\gamma = 1$, and $C = \mathcal{P}$ exactly. However, in the case of solid-state emitters, where typically $\gamma_0/\gamma \ll 1$, a cQED system can have a Purcell factor $\mathcal{P} > 1$ but still be in the regime $C < 1$. There are scenarios where this intermediate regime can offer useful enhancements. For highly broadened emitters ($\gamma \gg \kappa$), such as diamond defects at room temperature, the cavity can funnel otherwise broadband emission into the relatively narrow resonator mode, creating a frequency-tunable source of narrow-band single photons [108,112,127–129]. More typically, low-temperature solid-state cQED systems operate in the $\kappa \gg \gamma$ limit, with emitters still dominated by pure dephasing $\gamma_d \gg \gamma_0, \gamma_1$. In this case, the brightness of the optical transition of interest is enhanced by $\mathcal{P}$, and when Γ becomes larger than $\gamma_1 + \gamma_0$, the lifetime of the emitter begins to decrease significantly, increasing the overall rate of photon emission. However, as long as $C < 1$, the emitter linewidth is still determined primarily by γ_d, requiring detection during a short time window $\delta t \sim 1/\gamma_d$ to render the photons indistinguishable [130,131]. Nevertheless, as the cavity-coupling rate Γ increases, so does the probability of photon emission within δt. Hence Purcell-enhanced emission, in combination with spin-selective optical transitions [132–138], coherent qubit manipulation [102,132], and efficient outcoupling [107,139,140], could already greatly enhance the rate of remote entanglement generation [53,58,62,98,99,101].

In contrast, the high cooperativity regime $C > 1$ corresponds to conditions of near-deterministic interactions, where the emitter has a high probability to interact with a cavity photon before it dephases. High cooperativity is a prerequisite for protocols involving deterministic, cavity-mediated quantum information processing with spins and photons [27,46,78]. For example, in the high-cooperativity regime, single, indistinguishable cavity photons can be generated on demand [29]. Since this interaction is coherent and reversible, single photons injected into the cavity can also be completely absorbed by the emitter, enabling transduction of quantum states from light to matter [25,27,141]. Alternatively, the spin state of a single quantum emitter can fully modulate the amplitude or phase of a photon reflected from the cavity, enabling deterministic interactions with (or among) transient photons [46,142,143]. Finally, strongly coupled cavity photons can be used to mediate spin–spin interactions in a cavity or between distant, resonant cavities, enabling implementation of near-deterministic distributed quantum logic operations [9,26,27,144,145]. Notably, the efficiency and fidelity of such near-deterministic protocols can generally be improved by increasing C, motivating the development of cQED systems that can reach $C \gg 1$ [78].

A final consideration in cavity engineering is the efficient in- and out-coupling of light. In particular, the cavity-confined mode must be engineered to critically or over couple into a propagating mode that can be guided into a single-mode fiber with high efficiency [Fig. 1(a)]. This is equivalent to the condition $\kappa_c \geq \kappa_s$, where $\kappa_c + \kappa_s = \kappa$ and κ_c and κ_s are the cavity leakage rates into the collected and scattered modes, respectively. Beyond ensuring efficient photon collection, $\kappa_c \geq \kappa_s$ is a prerequisite for certain deterministic quantum logic operations between spins and photons [46,78]. Once coupled out of the cavity via κ_c, the photons should be mode matched with high overlap η into a single-mode fiber, either for detection or for distribution to distant quantum network nodes.

In summary, in order to achieve high cooperativity, the coherent interaction between the emitter and cavity photons must be made stronger than all decoherence mechanisms by maximizing

the ratio Q/V while minimizing undesirable dephasing $\gamma_1 + \gamma_d$. Accomplishing this is a central challenge of experimental cQED, and requires careful consideration of both cavity and emitter properties.

3. CHOOSING AN EMITTER

There exist a multitude of crystallographic defects with optical transitions within the bandgap of diamond [92], some of which have optically accessible spin degrees of freedom. An important class of defects comprises an impurity atom and single vacancy [150], of which the most studied are the negatively charged NV [Fig. 2(a)] and negatively charged SiV centers [Fig. 2(d)]. In addition, several emerging color centers have recently gained traction in the field, such as the neutral charge state of the SiV (SiV0), as well as negatively charged group-IV defects based on heavier impurities such as the germanium-vacancy (GeV), tin-vacancy (SnV), and lead-vacancy (PbV) centers. An ideal emitter for quantum information applications would combine deterministic fabrication with coherent, bright optical transitions that couple to long-lived spin states. This section provides a survey of such properties as well as other experimental considerations that are relevant in choosing a color center.

A. Fabrication

Efficient cavity coupling requires accurate emitter placement within the cavity mode as well as high optical coherence. Simultaneously achieving these requirements poses a significant challenge, and has spurred development of advanced techniques for emitter creation [151].

The best placement accuracy is obtained using ion implantation and annealing [152–154]. Standard blanket implantation forms a two-dimensional layer of impurities at a depth determined by the acceleration energy [155], while three-dimensional precision can be achieved using a focused ion beam (FIB) [156–159], or via blanket implantation through a lithographically aligned mask [160–163]. Combining shallow masked implantation and diamond overgrowth [164] could further aid 3D localization by limiting implantation straggle. Subsequent high-temperature, high-vacuum annealing repairs lattice damage and mobilizes vacancies to form the desired color center with sub-unity conversion efficiency [153,165,166]. Particularly for larger implanted species, annealing at higher temperatures (>1200°C) or pressures may be important to mitigate unwanted defects formed due to implantation damage [167,168].

In contrast to implantation, fabrication techniques based on as-grown impurities offer less control over position but generate defects with better optical properties. This was clearly illustrated by a recent study comparing as-grown and implanted NV centers in the same sample, where the former displayed superior optical coherence [Fig. 2(b) [147]]. As-grown NV centers can be formed using the non-negligible native nitrogen impurity levels present in electronic-grade diamond. Other impurities can be introduced in high-pressure, high-temperature (HPHT) [169–171] or chemical vapor deposition (CVD) diamond synthesis [172,173], and delta-doping techniques have been used to further localize emitters into a single layer [174,175]. In addition, precise boron doping has been critical in engineering the Fermi level of diamond to stabilize the SiV0 charge state [103]. Following impurity incorporation, techniques such as electron irradiation [176–178] or laser writing [179] can be used to generate vacancies, which, upon annealing,

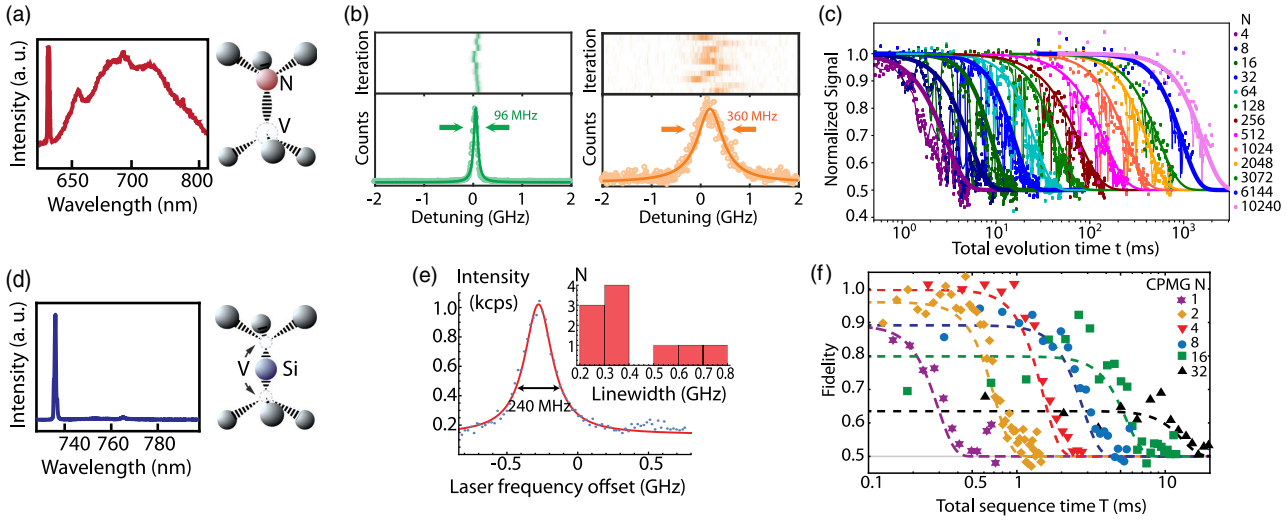

Fig. 2. (a) NV center structure and low-temperature emission spectrum (spectrum adapted with permission from Ref. [146], copyright Wiley-VCH Verlag GmbH & Co. KGaA). (b) Representative NV photoluminescence excitation (PLE) data at 4 K for each nitrogen isotope (green: ^{14}NV; orange: ^{15}NV). The sample is implanted with ^{15}N, and the ^{14}N are as-grown impurities. Individual scans of the ZPL reveal the linewidth free from spectral diffusion. The summation of many repeated scans shows spectral diffusion (adapted with permission from Ref. [147], copyrighted by the American Physical Society). (c) Decoherence of an NV electronic spin at 3.7 K with tailored decoupling sequences employing pulse numbers from N = 4 to N = 10,240 (adapted with permission from Ref. [148] in accordance with creativecommons.org/licenses/by/4.0/legalcode). (d) SiV center structure and low-temperature emission spectrum. (e) Linewidth of a representative implanted SiV at 4 K inside a nano-waveguide measured by PLE spectroscopy (blue points: data; red line: Lorentzian fit). Inset: histogram of emitter linewidths in nanostructures. Most emitters have linewidths within a factor of four of the lifetime limit (94 MHz) (adapted with permission from Ref. [149], copyrighted by the American Physical Society). (f) Spin coherence of an SiV electronic spin at 100 mK using CPMG sequences with N = 1, 2, 4, 8, 16, and 32 pulses. The longest measured T_2 time is 13 ms for N = 32 (adapted with permission from Ref. [102], copyrighted by the American Physical Society).

can combine with implanted or as-grown impurities to form emitters.

B. Optical Properties

Cavity-coupled quantum information technologies require a high rate of emission on a coherent optical transition. For diamond defects, such transitions lie within the ZPL. Moreover, to eliminate thermal broadening of the ZPL itself, experiments must be conducted at cryogenic temperatures (typically at ∼10 K or below [180,181]). The ZPL radiative emission rate (γ_0) is determined by a combination of the excited state state lifetime (τ), Debye–Waller factor (ξ), and quantum efficiency (QE) according to

$$\gamma_0 = \frac{\xi}{\tau}\mathrm{QE}, \tag{4}$$

neglecting for simplicity any fine structure within the ZPL (see Table 1 for a comparison of emitter properties). While emitter lifetimes vary by less than an order of magnitude, the Debye–Waller factor, or the fraction of radiative emission that occurs within the ZPL, is much lower for the NV than for group-IV emitters [182,183]. This is due to a change in the NV electronic wavefunctions (or charge distributions) between the ground and excited states, such that photon emission is accompanied by a significant shift in nuclear coordinates.

Quantum efficiency refers to the radiative fraction of total excited state decay, which can also include direct phonon relaxation [180,190]. In general, QE is challenging to extract directly from emitter brightness due to confounding factors such as the presence of metastable dark states and imperfect calibration of collection and detection efficiencies. Instead, QE can be most precisely estimated by measuring the response of the emitter's excited state lifetime to a controlled change in the local photonic density of states [191]. This technique has been used to show that the NV QE is close to unity in bulk diamond [192]. Unfortunately, this method is not as precise for emitters with QE substantially less than one, since their lifetimes do not depend as sensitively on their local photonic environment. This is the case for the SiV center [149], which is believed to have QE ≈ 0.1 at 4 K (see supplementary material in [193]). Indeed, the SiV's relatively short and temperature-dependent lifetime of ∼1.6(1.0) ns at 4(300) K [180] is consistent with strong nonradiative processes. On the other hand, the GeV center has a slightly longer, temperature-independent lifetime of 6 ns that is very sensitive to its local photonic environment [186], and single GeVs can induce coherent extinction of waveguide transmission [121,186]. These measurements suggest a relatively high QE $\gtrsim$ 0.4. However, this estimate is in conflict with a QE < 0.1 extrapolated using detected count rates from GeV centers in bulk diamond [194]. There is even more uncertainty regarding the QE of other emerging color centers including the SnV, PbV, and SiV0; however, it is worth noting that photon count rates in experiments involving SnV and SiV0 are consistent with a high QE comparable to that of the NV center [103,167].

Table 1. Summary of Emitter Properties (see text for details)

Defect	Symmetry	ZPL Wavelength	DW Factor (ξ)	Lifetime (τ)	$\hbar\Delta_{GS}/k_b$ [a]
NV	C_{3v}	637 nm	0.03 [118]	11–13 ns [132,184]	N/A
SiV	D_{3d}	737 nm	0.7 [185]	1.6–1.7 ns (4 K) [172,166,176]	2.4 K [135]
GeV	D_{3d}	602 nm	0.6 [169]	6 ns [186]	7.3 K [186]
SnV	D_{3d}	619 nm	0.6 (5 K) [187]	4.5–4.8 ns [137,138]	41 K [167]
PbV	D_{3d} [b]	520–552 nm [188,189]	unknown	> 3 ns [188,189]	200–270 K [188,189]
SiV0	D_{3d}	946 nm	0.9 [103]	1.8 ns [103]	N/A

[a] Temperature corresponding to exponential suppression of phonon-induced spin dephasing.

[b] PbV symmetry is unconfirmed experimentally.

Another consideration in choosing an emitter is the ZPL emission frequency. Working at longer wavelengths simplifies nanofabrication by allowing larger feature sizes with lower sensitivity to surface roughness. Furthermore, the GeV, SnV, and PbV ZPL wavelengths occur in the 520-620 nm range, where it is challenging to obtain stable, high-power lasers.

In addition, resonant cavity coupling relies on the spectral stability of the emitter, which is strikingly different for the NV center compared to group-IV defects owing to their different symmetries. While all of these color centers occur along the ⟨111⟩ family of crystal axes, the nitrogen of the NV center sits in place of a missing carbon atom, resulting in a defect with C_{3v} symmetry. Its lack of inversion symmetry permits inequivalent electric dipole moments in the ground and excited states; consequently, the NV center ZPL frequency is strongly impacted by electric field noise on nearby surfaces, causing spectral diffusion, or variation in frequency over time, particularly when illuminated by the green light used to reinitialize the negative NV charge state [184,195]. This effect is especially severe for implanted NV centers in nanostructures, which typically exhibit spectral diffusion of many GHz, far beyond the ∼15 MHz lifetime limit [196], corresponding to significant dephasing γ_d. Encouragingly, NV centers formed from native nitrogen impurities and electron irradiation have achieved spectral-diffusion linewidths of <250 MHz in a few-micrometers-thick diamond membrane [114]. Moreover, by applying pulses of green light until the NV transition matches a desired frequency [196], the effects of pump-induced spectral diffusion can be mitigated, and the majority of single-scan linewidths are below 100 MHz in such membrane samples [114]. Conversely, the electric field sensitivity of the NV can be viewed as a resource for tuning the ZPL frequency via the DC Stark effect, which has been used to actively compensate for both spectral diffusion and spectral mismatch of different defects [197–199].

In contrast to the NV center, group-IV defects take a split-vacancy configuration described by the point group D_{3d}, which includes inversion symmetry, leading to a vanishing permanent electric dipole moment. Such defects are insensitive to surface noise to first order; indeed, both as-grown [172] and implanted [149] SiV centers can display nearly lifetime-limited linewidths, even in nanostructures [149,159] [Fig. 2(e)]. Other group-IV color centers such as the GeV [136,186], SnV [138], and SiV0 [103] exhibit similar spectral stability, although this has not yet been observed in nanofabricated cavities. The insensitivity of group-IV emitters to electric fields precludes Stark shift tuning of the ZPL frequency; instead, two-photon Raman transitions [193,200] and dynamic control of the strain environment [201,202] are promising approaches for wavelength tuning and spectral stabilization.

Finally, it is desirable to minimize inhomogeneous broadening, or the variation in ZPL emission frequency from emitter to emitter. The inhomogeneous distribution scales with implantation damage, increasing with the size and energy of the ion, but can be mitigated to varying degrees via post-implantation treatment. NV and SiV centers can exhibit inhomogeneous linewidths down to 0.17 nm [154] and 0.03 nm [149], respectively, when annealed at high temperatures. Much larger linewidths of 30 nm have been observed for implanted SnV centers [138], although subsequent HPHT annealing was shown to achieve distributions down to 6 nm [167]. Furthermore, the spectral features attributed to the PbV ZPL around 520 nm exhibit a narrow distribution of only 0.12 nm; however, unidentified emission lines over a ∼100 nm range could be evidence of a much larger inhomogeneous distribution or intermediate defect formation [188], meriting further investigation. In practice, it is likely that a combination of improved inhomogeneous broadening and spectral tuning will be necessary to realize spectrally indistinguishable emitters.

C. Spin Properties

Many quantum information applications rely on spin–photon transduction via state-selective optical transitions within the ZPL [132,134,136–138]. These spin states, in combination with proximal nuclear spins coupled by magnetic dipolar interactions, can serve as an additional resource for storing or processing information [203] and performing local error correction [204].

In practice, the NV and SiV0 spins are easiest to work with due to their orbital singlet, $\mathcal{S} = 1$ ground states. A spin qubit can be realized between the $m_s = 0$ and either of the $m_s = \pm 1$ spin states, which are naturally separated in energy by a zero-field splitting. Coherent spin manipulation can be achieved via microwave fields [205], and NV centers have demonstrated the longest coherence times for a single electron spin qubit in any system ($T_2 > 1$ s) [Fig. 2(c)] [148]. So far, only ensemble spin resonance has been demonstrated for the novel SiV0 center; nevertheless, these defects display coherence times as long as $T_2 = 255$ ms at 4 K [103,206,207].

In contrast, color centers based on negatively charged group-IV defects exhibit a doubly degenerate ground state in both orbit and spin ($\mathcal{S} = 1/2$), with orbital degeneracy lifted by Δ_{GS} due to a combination of spin–orbit interaction and dynamic Jahn–Teller effect [135,208]. In an external magnetic field aligned with the ⟨111⟩ axis, the lowest energy spin-1/2 manifold can be addressed using highly cycling, spin-selective optical transitions [134,135,209,210]. The major challenge in working with the spins of negatively charged group-IV defects is rapid ground-state dephasing caused by single-phonon transitions between orbital states. This motivates qubit operation at temperatures well below $\hbar\Delta_{GS}/k_B$ (see Table 1) to reduce phonon occupation, thereby exponentially increasing spin coherence times. As a result, the SiV exhibits a four to five order-of-magnitude increase in spin coherence times at $T < 500$ mK [$T_2 > 10$ ms [102], Fig. 2(f)] compared to 4 K ($T_2 \sim 100$ ns [211]). A complementary approach for improving spin coherence involves increasing the ground-state splitting through the application of strain [201,212]. For instance, strain tuning of SiVs in nanostructures has demonstrated an order-of-magnitude increase in orbital splitting, resulting in the highest reported SiV coherence time at 4 K of $T_2 = 250$ ns [212]. Moreover, defects based on heavier group-IV ions exhibit larger Δ_{GS}, which could facilitate operation at higher temperatures. Indeed, the PbV orbital splitting is estimated to be in the THz regime, suggesting the possibility of long-lived spin coherence at 4 K [188,189].

A final consideration is the ability to couple to proximal nuclear spins of either the defect impurity or ^{13}C carbon isotopes in diamond. Impressively, the NV center has been used to control a 10-qubit quantum register with coherence times of > 75 s [93]. Single-site nuclear spin manipulation has also been demonstrated with the SiV [104,122], but multi-nuclear-spin registers have not yet been realized.

D. Discussion

Thus far, state-of-the-art cavity experiments with diamond defects have used either the NV or SiV. While the NV center is the best understood defect, exhibiting excellent spin coherence, its optical properties are poor. In particular, the difference in permanent electric dipole moments between the ground and excited states degrades optical coherence for near-surface emitters. Open Fabry–Perot microcavities containing bulk-like diamond membranes are therefore especially promising for these color centers, as they can be situated far from interfaces (see Section 4). In contrast, the SiV has poor spin properties at 4 K, requiring operation at dilution refrigerator temperatures to realize a long-lived spin qubit, but has superior optical coherence. Crucially, its inversion symmetry inhibits sensitivity to surfaces, allowing for incorporation into heavily fabricated nanoscale resonators with high Q/V (see Section 5).

In addition, we discussed the potential of emerging group-IV color centers. Negatively charged group-IV emitters based on larger ions appear to share the attractive optical properties of the SiV with the added potential for improved spin coherence times at 4 K, although these emitters are harder to fabricate and are not as well understood. The recently discovered SiV0 could potentially combine excellent optical and spin properties at liquid helium temperatures, but it requires specially doped diamond to stabilize the neutral charge state and is one of the least explored of the defects considered here. Finally, recent progress in *ab initio* [208,213,214] and machine learning [215,216] techniques suggests it may soon be possible to predict new emitters with properties superior to those discussed in this section.

4. OPEN FABRY–PEROT MICROCAVITIES

Early cQED experiments were performed using cm-scale Fabry–Perot cavities with Gaussian modes defined by two spherical mirrors [21,217]. Such cavities take advantage of absorption-limited dielectric mirror coatings to achieve very high reflectivity [218,219], and offer full spatial and spectral tunability by positioning the mirrors, but their cm-scale size leads to large mode volumes and limited scalability. By miniaturizing the spherical mirrors, these drawbacks can be mitigated, with micrometer-scale geometries achieving mode volumes on the order of λ^3 [220]. Moreover, the small size of the micromirrors enables parallelized fabrication processes [220–222] and direct integration with optical fibers [107,223].

So far, open microcavities have been coupled to a multitude of quantum systems including atoms [224], ions [82,225], molecules [80,226], quantum dots [227], rare earth ions [228], optomechanical systems [229], and color centers in both nanodiamonds [108–112,127] and diamond membranes [129,230–232]. Early

results with diamond defects utilized nanodiamonds containing single NV centers at elevated temperatures [108–110] to observe funneling of the broad emission into the narrow resonator mode (see Section 2). However, NVs in nanodiamonds are poorly suited to spin–photon interfaces, as their optical properties are degraded by nearby surfaces, motivating the development of a membrane-in-cavity geometry in which emitters can exhibit coherent optical transitions at 4 K [114]. Nevertheless, despite substantial progress in both mirror and diamond fabrication, obtaining $C > 1$ for a color center in a membrane-in-cavity system has not yet been achieved. In this section, we outline the theoretical and experimental progress toward this goal, followed by a near-term outlook for the field.

A. Geometry

For coupling to defects in a diamond membrane, most experiments employ a half-symmetric geometry [Fig. 3(a)] formed by a macroscopic flat mirror and a microscopic spherical mirror with radius of curvature R, fabricated either on the tip of an optical fiber or planar substrate [Fig. 3(b)]. Diamond defects are contained within a membrane of thickness t_d bonded to the flat mirror. The spacing between the spherical and flat mirrors determines the cavity length L.

As discussed in Section 2, it is desirable to obtain a high ratio of cavity quality factor Q to mode volume V. The mode volume is $V \approx \pi\omega_0^2 L_{\text{eff}}/4$, where ω_0 is the cavity waist, and L_{eff} is the effective cavity length expressed in terms of an equivalent distance in diamond [233], $L_{\text{eff}} = (2/n_d^2|E_d|^2)\int_{\text{cav}} n^2(z)|E(z)|^2 dz$. Here, $n(z)$ and $E(z)$ are the refractive index and electric field at position z in the cavity, and n_d and E_d are the index and maximum electric field in diamond, respectively. In principle, Q/V can be largely independent of L_{eff} because the photon lifetime—and thus Q—typically increases linearly with cavity length when losses occur at mirrors and interfaces. Consequently, the figure of merit becomes

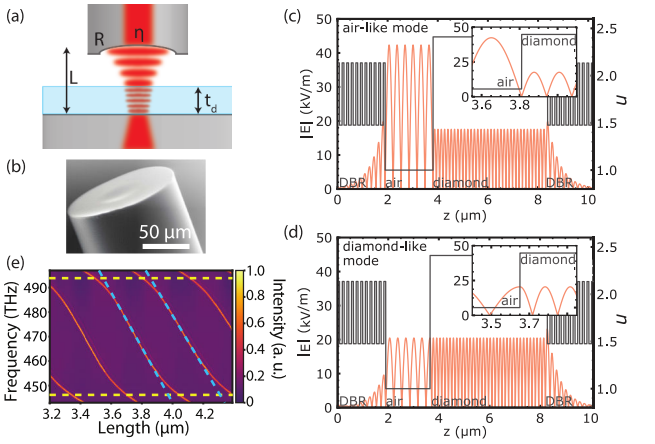

Fig. 3. (a) Schematic of a fiber cavity (adapted with permission from Ref. [113], copyrighted by the American Physical Society). (b) Scanning electron microscope (SEM) image of a laser-machined fiber tip (adapted with permission from Ref. [107], copyrighted by IOP Publishing and Deutsche Physikalische Gesellschaft, reproduced by permission of IOP Publishing, CC BY-NC-SA). (c), (d) Refractive index n (black, right axis) and electric field strength (orange, left axis) for (c) an air-like mode and (d) a diamond-like mode (adapted from Ref. [233] in accordance with creativecommons.org/licenses/by/3.0/). (e) Membrane-in-cavity mode structure, exhibiting large avoided crossings between diamond (yellow) and air (blue) modes (adapted with permission from Ref. [129], copyrighted by the American Physical Society).

$Q/V \propto \mathcal{F}/(\lambda\omega_0^2)$, where the finesse $\mathcal{F}$ is π divided by the effective per-pass losses in the cavity. Nevertheless, in practice, it is easiest to simultaneously achieve a small waist ω_0 and high finesse $\mathcal{F}$ using short microcavities (see discussion of losses below). Consequently, maximizing Q/V for open-geometry cavities typically involves minimizing losses and reducing R (since $\omega_0 \propto \sqrt{R}$ for $R \gg L$), as well as L, t_d, and electric field penetration into the mirror coatings.

A final geometric consideration is collection efficiency, which is determined by the overlap η between the transmitted cavity electric field and that of a single-mode fiber. Micromirrors fabricated on planar substrates allow introduction of optical elements to maximize fiber coupling of outcoupled light [234], but in turn require challenging optical routing in a cryostat, although novel alignment techniques may alleviate some of this difficulty [235]. In contrast, mirrors fabricated directly on the tips of optical fibers feature direct coupling from the cavity to the propagating fiber mode. This coupling is maximized by precisely centering the mirror on the fiber core, while matching the fiber and cavity mode diameters and minimizing wavefront curvature [107,236]. For such cavities, there exists a trade-off between obtaining a small mode waist (requiring small R) and maximizing η due to wavefront curvature mismatch. Nevertheless, power coupling efficiencies of $\eta^2 > 85\%$ have been demonstrated with empty fiber cavities [107].

B. Mode Structure

The diamond membrane strongly modifies the cavity mode structure and losses compared to those of an empty or "bare" cavity. This behavior is well captured by a simplified one-dimensional model of the cavity electric field with nodes at the mirror interfaces [113,233]. The field at the air–diamond interface is therefore completely determined by the membrane thickness t_d, which sets the relative energy density in the air and diamond regions via the electromagnetic boundary conditions. A field node at this interface leads to an "air-like" mode, where the intensity is higher in the air versus the diamond region by a factor of n_d [Fig. 3(c)], while an anti-node leads to a "diamond-like" mode where the opposite is true [Fig. 3(d)].

The mode types are readily identified from cavity transmission spectra [Fig. 3(e)]. The canted periodic structure can be understood by considering the limit of a perfectly reflective air–diamond interface (i.e., $n_d \to \infty$), in which case the cavity is divided into "air" and "diamond" modes [blue and yellow lines in Fig. 3(e)]. The frequency spacing of these modes depends on the diamond thickness and cavity length according to $\Delta\nu_{\text{di}} = c/(2n_d t_d)$ and $\Delta\nu_{\text{air}} = c/(2(L - t_d))$. With finite n_d, these modes are coupled to one another, leading to the large avoided crossings observed in the spectrum, where diamond-like modes have a shallow slope, and air-like modes have a steeper slope [113]. The sensitivity of field localization to frequency and diamond thickness offers an extra layer of tunability to the open-cavity geometry.

Based on available mirrors, open cavities can in principle achieve an extraordinary finesse of $\sim 10^5$ or more [218,219]. In practice, it is very challenging to achieve such high values in membrane-in-cavity systems. Losses due to scattering or absorption at the air–diamond interface display exquisite sensitivity to the field amplitude at this position; such losses are consequently maximized for diamond-like modes and minimized for air-like modes [113]. Models including known surface roughness [113,233] exhibit smaller surface losses than seen in experiments [113,230],

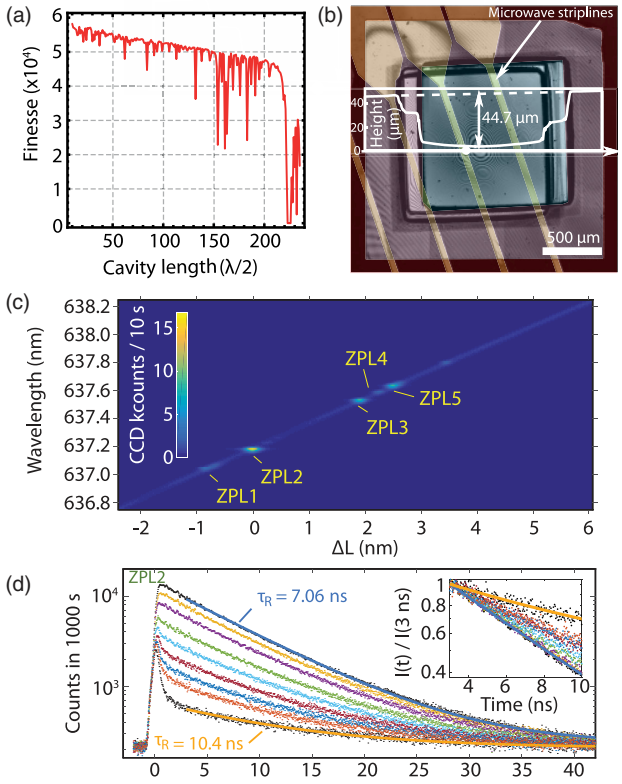

Fig. 4. (a) Cavity finesse as a function of axial mode order. Drops in finesse arise from perturbative coupling to lossy higher-order modes caused by the Gaussian shape of fiber mirror (adapted with permission from Ref. [239] in accordance with creativecommons.org/licenses/by/3.0/). (b) Confocal microscope image of an etched diamond membrane with false color added. The white arrow indicates the path along which the height profile was measured (adapted with permission from Ref. [114], further permissions related to the material excerpted should be directed to the ACS). (c) PL spectra around the NV ZPL transition frequency for different air-gap detunings ΔL. Each resonance corresponds to the ZPL emission of a single defect. (d) Photoluminescence decay curves of "ZPL2" from (c) following pulsed excitation at different cavity lengths. The inset shows the normalized decay curves corresponding to a reduction in lifetime from 12.6 to 7.06 ns (parts (c) and (d) were adapted with permission from Ref. [230] in accordance with creativecommons.org/licenses/by/4.0/legalcode).

indicating significant contributions from absorption at the diamond surface. In contrast, bulk membrane absorption can be neglected for electronic grade samples [237].

Other sources of loss stem from non-ideal cavity geometry, as the finite extent of the micromirror can lead to clipping losses for large mode diameters (which increase with cavity length) [107]. Such losses are exacerbated when the cavity mode couples to higher-order transverse modes, which can result from deviation of the micromirror from an ideal spherical shape [238] [Fig. 4(a)] and deviation of the flat mirror from an ideal plane [239].

C. Fabrication

Scalable quantum technologies based on open microcavities require deterministic and repeatable fabrication processes for both the micromirror and diamond membrane. Micromirror fabrication seeks to produce shallow parabolic dimples with micrometer-scale radius of curvature, while maintaining nearly atomically smooth surfaces compatible with high-finesse dielectric coatings. So far, the most popular methods for machining mirror templates are based on laser ablation, FIB, and silicon etching. Laser ablation using a CO_2 laser results in controlled creation of Gaussian-shaped dimples with low surface roughness (0.2 nm-rms) [240–242]. Recently, the inclusion of additional nanofabrication steps achieved an effective $R < 5$ μm (based on the frequency spacing between higher-order transverse modes), with ablation depths of only ≈ 1 μm [243]. In contrast, FIB milling has been used to fabricate dimples with very small radii of curvature and precisely controlled geometry at the expense of higher surface roughness (0.3 − 0.8 nm-rms [109,221,244]). This method produced dimples with effective $R = 4.3$ μm and depths of only 230 nm [244]. Finally, silicon etching has been used to generate large arrays of ultra-smooth (0.2 nm-rms) mirror templates [245,246]. So far, this technique has produced relatively large radii of curvature ($R > 100$ μm), but smaller geometries may be possible. Once fabricated, mirror substrates are subsequently coated with low-loss dielectric mirrors. After deposition, it is possible to integrate microwave striplines for spin control directly into the flat mirror substrate while maintaining a high cavity finesse [247] [see Fig. 4(b)].

The second fabrication requirement is a process capable of producing ultra-smooth, micrometer-thick diamond membranes containing individual defects with bulk-like optical properties. The starting point for such a membrane is typically a commercially available ∼100 μm thick electronic grade diamond plate. Etching hundreds of micrometers to obtain a single membrane constitutes a long and wasteful process; consequently, membrane substrates are generally obtained from bulk samples by either laser slicing and polishing (resulting in $t_d \sim 10$ μm) or via a novel implantation process [232,248]. The latter technique involves implanting He atoms to form an amorphous subsurface layer, which is converted to graphite by subsequent annealing. The diamond is then overgrown with pristine single-crystal diamond, and released at the graphitic layer with electrochemical etching, yielding $t_d \sim$ 100 nm −1 μm. Both techniques produce a surface roughness of a few nm, but thus far membranes based on laser-sliced substrates have achieved the best results for surface losses [129] and fabrication of individually addressable defect centers [114,129,230] (see Section 3). Membrane substrates can then be bonded to carrier wafers via van der Waals forces for further processing. Thinning and smoothing of both surfaces is achieved through an inductively coupled plasma reactive ion etching (ICP RIE) process, which cycles between $ArCl_2$ and O_2-based recipes [249–252], obtaining a final surface roughness as low as ∼0.1 nm − rms [253]. Once the desired device thickness is achieved, the sample can be transferred using a micromanipulator [230] or in a water droplet to the flat mirror substrate. Recent results show that it is also possible to conduct the final etch through a quartz mask after bonding the sample to the mirror, reducing membrane handling [114] [Fig. 4(b)].

D. State of the Art

Despite considerable experimental progress, there has been only one demonstration of a single emitter in a diamond membrane coupled to an open microcavity at low temperature [230]. In this experiment, an implanted NV center was coupled to a $\mathcal{F} = 5{,}260$ air-like mode [Fig. 4(c)] resulting in a ZPL enhancement of $\mathcal{P} \approx 30$, an excited-state lifetime reduction by a factor of 2.0, and 46% of photons emitted into the ZPL. Furthermore, the tunability

of the system was illustrated by a variation in excited-state lifetime as a function of cavity length [Fig. 4(d)]. While this experiment represents a major milestone in coupling open cavities to diamond defects, it achieved an estimated cooperativity of only $C \approx 0.03$. This value is strongly impacted by an increase in spectral diffusion from 100 MHz to 1 GHz associated with thinning the membrane to $t_d < 1$ μm, and could potentially be improved by an order of magnitude by using a slightly thicker sample containing NVs formed by native nitrogen and electron irradiation [114,147] or by using more stable group-IV defects. Furthermore, reduced losses at the diamond interface would increase the cavity finesse and permit coupling to diamond-like modes. Such improvements recently led to the coupling of a single GeV center to a finesse 11,000 diamond-like mode of an open microcavity [129]. Finally, cavity mode volume could be reduced by decreasing the mirror radius of curvature using a combination of laser ablation and nanofabrication techniques [243].

Beyond fabrication, there are additional technical barriers limiting emitter–cavity coupling strength. Resonant coupling requires stabilization of the cavity length to well within a linewidth, on the order of 10 pm for state-of-the-art mirrors. For instance, the liquid helium cryostat used in the aforementioned NV experiment induced vibrations of 24 pm-rms in the passively stabilized cavity, representing a significant fraction of the 60 pm cavity linewidth [254]. Consequently, many avenues for increasing stability have been explored such as rigid mounting [236], external vibration isolation [255], thermal feedback of the mirror coatings [236,256], as well as active locking methods such as Pound–Drever–Hall [236,257], side-of-fringe [232], and Hänsch–Couillaud techniques [80,258].

E. Outlook

Recent experimental milestones suggest that it should soon be possible to couple bulk-like emitters in diamond membranes to high-finesse open microcavities. This is particularly promising for achieving $\mathcal{C} > 1$ for an NV center, which has been a long-standing challenge due to the degradation of emitter optical properties in nanofabricated resonators (see Section 5). Furthermore, the narrow cavity linewidths afforded by open cavities offer an opportunity for spin-selective enhancement, opening the door for high-fidelity spin measurement [259], as well as schemes for quantum communication, computation, and metrology [10,260,261]. Finally, while scaling to multi-cavity systems remains an active area of research [262], progress in parallelized open-cavity fabrication techniques [222] shows the potential for larger-scale technologies.

5. NANOPHOTONIC CAVITIES

In contrast to open-geometry cavities, nanophotonic resonators can readily achieve sub-micrometer mode volumes by using refractive-index contrast to confine light to volumes of order $(\lambda/n)^3$ or smaller [263–266]. Additionally, nanophotonic structures are naturally desirable for long-term scalability, since they can be fabricated en masse and utilize on-chip photon routing [267,268]. For a general, platform-agnostic overview of nanophotonic systems, we direct the reader to an alternate review [269].

With its high index of refraction $n = 2.4$, diamond is a natural candidate for such systems, and in the absence of scattering or absorption losses, diamond nanophotonic resonators could theoretically achieve $\mathcal{P} \sim 10^5$ [270], or $Q/V_0 > 10^6$, where $V_0 = V(n/\lambda)^3$ is the mode volume relative to a cubic wavelength in the diamond. A wide variety of cQED structures have been fabricated in diamond [271], including whispering gallery mode resonators [272,273], ring resonators [116,274], and photonic crystal cavities (PCCs) [115,275–277]. Here, we focus on the unique technical considerations involved in realizing and utilizing nanophotonic structures for cQED in single-crystal diamond, and related experimental progress therein.

A. Fabrication Techniques

The typical approach for nanoscale fabrication of high-quality photonic devices begins with single-crystal thin films (∼100 nm) grown heteroepitaxially, such as silicon-on-insulator, which can then be processed into undercut photonic structures using standard lithography and wet-etching techniques [278]. Unfortunately, this relatively straightforward approach to engineer optically isolated photonic structures does not translate effectively to the fabrication of diamond. Despite immense progress in the field of diamond growth, heteroepitaxial single-crystal thin films of diamond cannot yet be produced with defects at or below the parts-per-billion level, as required for quantum optical experiments involving single emitters [279–283]. Additionally, diamond is resilient to all forms of wet etching. Instead, less controllable plasma-based dry etching techniques [284] must be used in combination with sophisticated lithography masks [272,285]. Initial successes in nanofabrication of diamond [e.g., see Figs. 5(a) and 5(b)] overcame these challenges using creative techniques to engineer nanoscale diamond membranes with sub-micrometer thickness, either via ion-beam implantation and liftoff or mechanical polishing and subsequent reactive-ion-etch thinning, but both techniques struggled with low resulting cavity and emitter quality [274,275,286–289].

Rather than membrane-based fabrication, underetching of structures defined in bulk, electronic-grade, single-crystal substrates [291] has recently enabled high-quality nanophotonic devices [Figs. 5(c)–5(m)]. Unlike most nanoscale membrane structures, devices undercut from bulk substrates can achieve high quality factors due to their optical isolation from the bulk, and are compatible with annealing and acid-cleaning post-processing steps required for incorporation of high-quality single emitters (Section 3). Underetching was first implemented by using an angled etch to undercut one-dimensional structures predefined with electron-beam lithography and top-down etching, leaving behind freestanding diamond nanobeams with triangular cross sections [Fig. 5(h), steps I–III]. The angled etch was initially accomplished by placing samples inside a triangular Faraday cage within the reactive-ion etcher [270,292]. More recently, a similar angled etch has been achieved using ion-beam milling at a well-controlled angle of incidence, resulting in more reliable etch profiles [293]. Both of these techniques have proven extremely effective for fabricating freestanding one-dimensional PCCs out of electronic-grade diamond substrates, such as those shown in Figs. 5(c)–5(i), with high ratios of $Q/V_0 > 10^4$ [123,270].

Underetched devices can also be fabricated out of bulk single-crystal diamond using a selective crystallographic etch to achieve a flat lower surface, as illustrated in Fig. 5(l) [272,294]. This etching technique was initially developed to fabricate high Q/V_0 whispering gallery mode resonators [Fig. 5(m)] [272,273], and has now been adapted to fabricate freestanding PCCs with rectangular cross

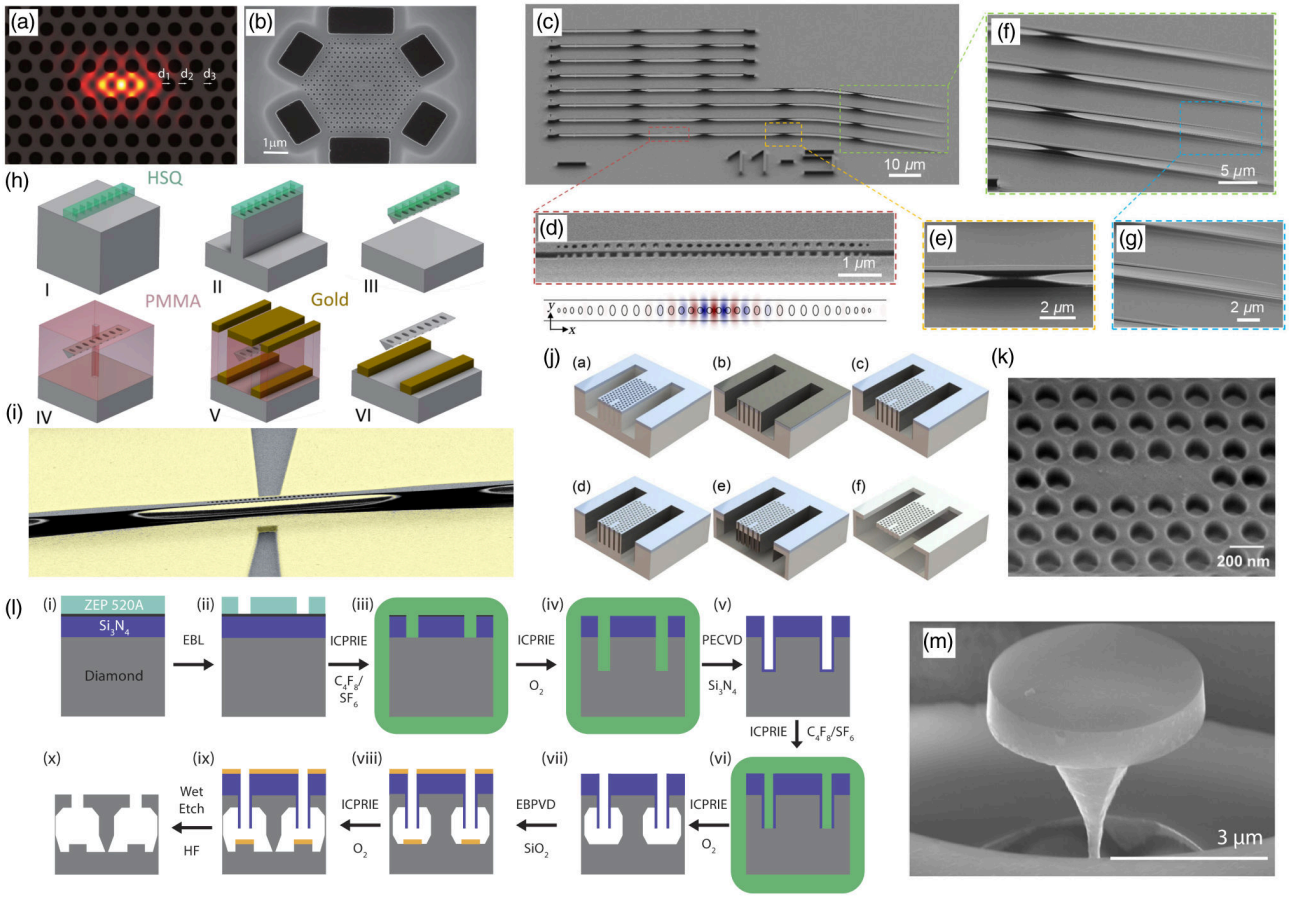

Fig. 5. Diamond nanophotonic devices. (a) Mode simulation and (b) SEM of 2D PCC fabricated from an ultra-thin diamond membrane (reprinted with permission from Ref. [286], copyrighted by the American Physical Society). (c) SEM of an array of freestanding PCCs created by angled reactive ion etching, highlighting (d) 1D PCC region, (e) support anchor connecting waveguide to substrate, and (f), (g) tapered waveguide region for adiabatic single-mode fiber coupling (reprinted with permission from Ref. [140], copyrighted by the American Physical Society. (h) Fabrication procedure for angle-etched devices (steps I–III), including targeted implantation through a mask (IV) and microwave electrode deposition (V–VI) (reprinted with permission from Ref. [123], copyrighted by the American Physical Society). (i) SEM of resulting devices with gold coplanar waveguide for microwave spin control (false color added, adapted with permission from Ref. [122], copyrighted by the American Physical Society). (j) Rectangular cross-section PCC fabrication procedure using an anisotropic crystallographic etch and (k) SEM of a freestanding 2D PCC (reprinted with permission from Ref. [290], AIP Publishing). (l) Optimized procedure to fabricate microdisk resonators using the crystallographic etch and (m) resulting high Q/V_0 device (reprinted with permission from Ref. [272], AIP Publishing).

sections [295], enabling two-dimensional PCCs in single-crystal diamond [Figs. 5(j)–5(k)] [290]. While the crystallographic-etch technique is somewhat less mature than the angled etch, it allows for rectangular device geometries similar to conventional photonic platforms. This should enable fabrication of waveguides with arbitrary relative spacing, allowing for implementation of freestanding diamond-waveguide-based beam splitters and electromechanical switches for on-chip photon routing [267,268]. Furthermore, this technique has a largely unexplored parameter space available, making it possible to optimize the mask and etching procedure to achieve a wide variety of surface properties [272,296].

In order to utilize low-mode-volume cavities for cQED experiments, color centers must be placed at the mode-field maximum of the cavity with sub-100 nm precision. This has been accomplished with SiV centers using a variety of techniques (Section 3), including delta doping [297], FIB implantation [157–159], and blanket ion implantation through lithographically aligned masks [160–162]. By implanting several ions and utilizing spectral selection of individual emitters, these techniques have enabled deterministic nanoscale PCC coupling of single SiV centers [122,193,298].

Once fabricated, nanoscale cavities can be optically interrogated using free-space optics [116,286] or a transient coupler such as a tapered fiber [270,299]. Coupling can also be made indirectly by means of a waveguide in which the PCC is integrated [e.g., see Figs. 5(c), 5(d), 5(i)]. In this case, the cavity design is adjusted to damp preferentially into the diamond waveguide mode (see Section 2, [263]), which can subsequently be outcoupled into a single-mode fiber by various techniques. Even a small defect in the waveguide, such as a deliberately introduced notch, induces scattering into free-space modes that can be coupled into a single-mode fiber via a high-numerical-aperture objective, albeit with limited $\eta^2 \sim 1\%$ efficiency [193,200,297]. Alternatively, grating structures [274,300] can enable $\eta^2 \sim 10\%$ coupling efficiency by improving mode matching, and can be made broadband using optimized photonic design principles [301].

Nanophotonic structures can also be directly integrated into single-mode fiber networks. This has been done extremely

efficiently using adiabatically tapered diamond waveguides coupled to similarly tapered optical fibers using van der Waals forces, yielding efficiencies close to unity [140,302]. Currently, this technique requires precise nanopositioning of the adiabatically tapered fiber, which can be challenging and costly to implement in cryogenic conditions where experimental access is limited [123,298]. Instead, permanent and efficient integration into large-scale photonic circuits will likely be necessary to scale up nanophotonic cQED experiments. The first steps in this direction have recently been demonstrated using a pick-and-place technique to integrate diamond structures with aluminium nitride photonic circuits, enabling access to group-IV color centers in 72 separate diamond nanophotonic waveguides [121].

B. Practical Considerations for Scalability

A high overall yield of devices usable as coherent spin–photon interfaces is necessary for quantum networking with several nodes [123,285]. Beyond deterministic incorporation of defect centers, the monolithic nature of nanofabricated diamond structures creates additional yield-limiting challenges for color center cQED experiments. Due to imperfections in device fabrication, the resonance wavelength of nanophotonic diamond cavities must be fine-tuned *in situ* in order to precisely match the low-temperature ZPL emission wavelength of an individual color center. Unlike the open Fabry–Perot cavity (Section 4), in which cavity frequency can be controlled by changing the cavity length, nanophotonic cavities cannot be tuned by mechanical displacement. Instead, diamond nanophotonic cavities have been tuned by condensing gas on the nanostructure at cryogenic temperatures [193,270,297,303], which increases the local index of refraction, red shifting the optical mode. This effect can then be reversed selectively and precisely by using laser light to boil away gas that has already been deposited, leading to a well-controlled net red shift of individual device frequencies by several percent of the resonance wavelength [123,298]. Although effective, this technique is relatively slow and adds significant experimental overhead in cryogenic engineering.

The ability to tune the emission frequency of a color center *in situ* is another requirement for integration into quantum networks (Section 3). Recent nanophotonics experiments have focused on group-IV color centers because they are relatively insensitive to electrical noise from nearby nanostructured surfaces. However, this electric field insensitivity means they also cannot be manipulated by DC Stark shifts. One successful approach has used two-photon Raman transitions to overlap the emission frequencies of two SiV centers that initially differed by several GHz [193]. When employed in combination with cavity coupling, such Raman transitions have enabled widely tunable, cavity-enhanced single-photon emission spanning the entire inhomogeneous distribution of the SiV center [200] [Figs. 6(e)–6(h)]. However, wideband tuning via the Raman approach requires driving fields with substantial strength that may introduce heating and charge instability [123,193]. Alternatively, color center transitions can shift with strain, and electro-mechanical tuning has recently enabled deterministic emitter resonance matching and active locking for compensation of spectral diffusion (reduction of γ_d) inside nanoscale diamond waveguides, two key criteria in building large-scale networks out of solid-state defects [202]. However, incorporating similar nanomechanical capacitors with freestanding diamond PCCs remains an outstanding challenge.

Incorporation into nanostructures also poses challenges for the spin degrees of freedom of defect centers, where long spin coherence times observed in bulk diamond [148] are reduced by nearby surfaces and impurities introduced by implantation and fabrication [253,305]. Furthermore, state-of-the-art coherence times are achieved using lengthy dynamical-decoupling pulse sequences that typically require power delivery on the scale of several watts [93,102,148,211,306]. Coherent spin control has been accomplished for NV centers inside diamond nanostructures in a helium flow cryostat [304]. However, in the case of SiV centers, experiments are typically limited by the sub-milliwatt cooling power of dilution refrigerators at 100 mK temperature [102]. Additionally, lattice strain is required to allow the magnetic dipole transition between spin states for group-IV color centers [102,123,135], reducing the yield of suitable emitters in devices without strain-tuning capabilities.

These challenges have prompted the use of lithographically aligned gold striplines in close proximity to the PCC [Fig. 5(i)]. Such devices have enabled high-fidelity coherent control of an SiV center and nearby ^{13}C nucleus with coherence times > 1 ms and > 100 ms, respectively, at millikelvin temperatures [122]. Despite this success, residual heating from microwave pulses is believed to limit operational fidelity [124], motivating the development of superconducting microwave striplines on diamond. As an alternative to microwave manipulation, all-optical spin control using two-photon transitions is possible [307,308]. However, such techniques have yet to yield control fidelities comparable to the microwave approach and have not yet been implemented in nanostructures, which may also be particularly susceptible to heating from optical control fields [309]. One final approach is coherent electromechanical driving, which has recently been accomplished using a piezoelectric surface acoustic wave actuator [310]. It is likely that some combination of advances in strain engineering and low-power, on-chip microwave electronics will be required to scale up diamond nanophotonic cQED experiments at cryogenic temperatures.

C. State of the Art

The first proof-of-principle experiments almost 10 years ago showed Purcell enhancement of NV and SiV ZPL transitions in nanophotonic resonators [116,277,286,304,311,312] [see Fig. 6(a) for an example]. However, these experiments were limited to the $C < 1$ regime due to emitter dephasing inside heavily fabricated structures, which remains an outstanding challenge for NV centers [286]. Instead, the use of environmentally insensitive SiV centers enabled pioneering experiments in the $C \gtrsim 1$ regime, which was experimentally verified using the coherent extinction of resonant transmission through the cavity [Fig. 6(b)], as well as radiative broadening of the SiV optical transition [193,297].

Technical improvements, including more accurate emitter positioning using lithographically aligned masks [123], more reliable angled-etch procedures using ion-beam milling [293], and operation at millikelvin temperatures to eliminate residual thermal decay and decoherence effects [102,193], have now enabled nanophotonic SiV cQED devices in the $C \gg 1$ regime [Fig. 6(c)], [124]. This has allowed the first experimental observation of photon-mediated interactions between two emitters inside a cavity using SiV centers [298] [Fig. 6(d)], offering a potential pathway towards deterministic quantum logic gates between color centers

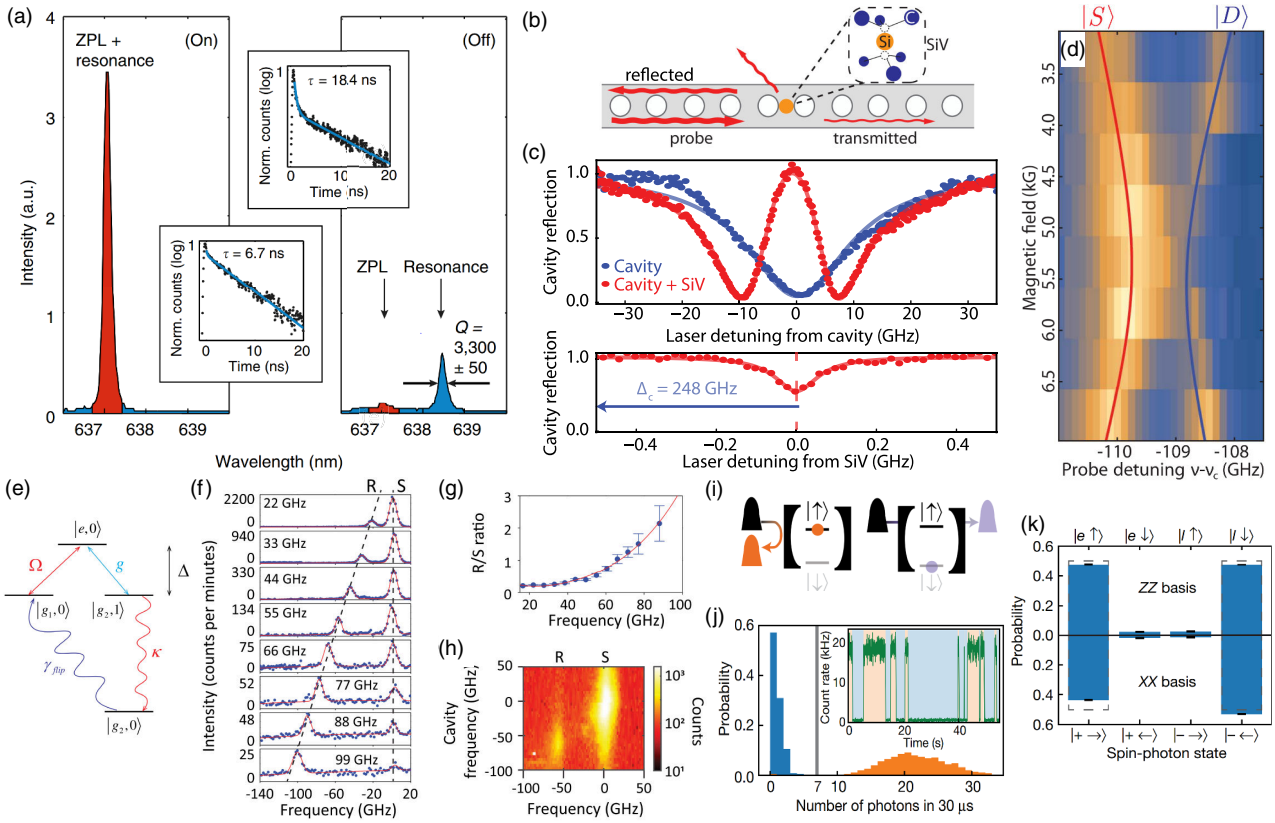

Fig. 6. State-of-the-art diamond nanophotonic cQED experiments. (a) Cavity enhancement of NV center ZPL, showing Purcell-reduced excited-state lifetime (reprinted from Ref. [304] in accordance with creativecommons.org/licenses/by/4.0/legalcode). (b) Schematic for characterizing nanophotonic SiV cQED parameters by coherent transmission and reflection from SiV–cavity system (reprinted from Ref. [193] in accordance with creativecommons.org/licenses/by/4.0/legalcode). (c) Strongly coupled SiV–cavity system (reprinted with permission from Ref. [124]). (Top) reflection spectrum of cavity without (blue, $\kappa = 21.6 \pm 1.3$ GHz) and with (red, $g = 8.38 \pm 0.05$ GHz) SiV coupling. (Bottom) natural linewidth measurement at large cavity detuning ($\gamma = 0.123 \pm 0.01$ GHz), yielding $C = 105 \pm 11$. (d) Coherent cavity-photon-mediated interaction between two SiV centers tuned into resonance using an external magnetic field (reprinted with permission from Ref. [298]). (e) Level structure and (f) experimental demonstration of cavity-enhanced SiV Raman emission over ∼100 GHz range, with Raman (R) and spontaneous (S) emission components labeled, (g), (h) showing transfer of emission spectrum from S to R under suitable cavity detuning (reprinted with permission from Ref. [200], copyrighted by the American Physical Society). (i) SiV spin-dependent cavity reflection (reprinted with permission from Ref. [122], copyrighted by the American Physical Society) enables (j) observation of spin quantum jumps and single-shot spin readout with fidelity $F = 0.9998^{+0.0002}_{-0.003}$ in 30 μs and (k) spin–photon entanglement with state fidelity $F \geq 0.944 \pm 0.008$ (reprinted with permission from Ref. [124]).

similar to those employed in superconducting microwave quantum processors [313]. Translation of these techniques to the optical domain will require further improvements in device cooperativity [78] along with implementation of optimized heralded schemes to overcome cavity loss [314].

Coherent spin–photon interfaces have been achieved by combining these high cooperativity devices with microwave spin control of SiV centers and nearby nuclear spins [102,122]. Additional technical advances, such as vector magnetic field control and precise optimization of SiV-cavity detuning, have given access to SiV spin states with high cavity reflection contrast and cycling transitions [Fig. 6(i)] [123]. These elements allow for extremely high-fidelity single-shot spin readout [Fig. 6(j)] and spin–photon entanglement [Fig. 6(k)] [124].

The current generation of diamond nanophotonic cavities are among the state of the art across all experimental platforms in several key quantum networking criteria: atom–photon cooperativity ($C > 100$) [124], spin coherence times ($T_2^{\mathrm{SiV}} > 1$ ms, $T_2^{^{13}C} > 0.2$ s) [122], spin readout and spin–photon entanglement fidelity ($F_r = 0.9998^{+0.0002}_{-0.0003}$, $F_e \geq 0.944 \pm 0.008$) [124], and emitter tunability (∼100 GHz) [200,202]. These developments have very recently culminated in the first experimental demonstration of a memory-enhanced quantum communication protocol [124]. Diamond nanophotonic cavities are now being used for implementation of novel protocols in quantum optics and information science reaching beyond the diamond photonics community, signaling the maturity of the field and its potential to play a prominent role in construction of quantum technologies.

D. Outlook

Despite immense progress in the field, diamond nanophotonics has yet to approach the peak of its potential. A number of outstanding challenges remain to be tackled. First, truly scalable fabrication will require development of wafer-scale quantities of thin-film diamond [279–283,315,316] for rapid and reliable processing into PCCs. Second, in the short term, current techniques for undercutting structures in diamond can still be improved, as quality factors of nanoscale PCCs are still limited by scattering losses introduced by imperfections in device fabrication [270,272]. Finally,

integration of diamond PCCs with more sophisticated nanophotonic circuits will be required to truly leverage the advantages of nanophotonics for large-scale systems [121,317]. Efficient incorporation of detectors [318,319], routing elements such as beam splitters and switches [267,268], control and tuning electronics [123,202], and frequency converters to telecommunications wavelengths [320,321] remain long-term goals for diamond nanophotonic cQED systems.

6. CONCLUSION

This review has considered two approaches for cavity coupling of diamond defects with complementary strengths. Fabry–Perot-style cavities offer compatibility with bulk-like defects, making them suitable for use with NV centers in currently available materials [114]. Moreover, their very high quality factors $> 10^6$ allow linewidths smaller than the fine structure splittings of the NV center, enabling the spin-selective cavity enhancement employed in proposed protocols for qubit readout and quantum networks [10,259,260]. Finally, cavity mirrors formed on the tips of optical fibers couple directly to propagating fiber modes, simplifying outcoupling. Diamond nanophotonic approaches, on the other hand, achieve nanoscopic mode volumes while maintaining good quality factors, leading to the strongest Purcell enhancements. While NV centers broaden problematically in such structures, the SiV retains good optical coherence, and newer defects may prove similarly insensitive to nanofabrication [87]. The different capabilities of the two platforms make them suited to complementary goals in quantum information science.

In the longer term, both cavity platforms will require improvements and additional capabilities to realize practical applications of quantum networks. Many technical challenges require further attention, including inhomogeneous broadening on emitter optical transitions and intra-cavity control over spins. Beyond improving the properties of the cQED platform itself, other advances will be needed to incorporate them into quantum networks. Since diamond defects emit primarily in the visible and NIR, conversion to telecom wavelengths will be necessary for long-distance networks. Already, 17% conversion efficiency has been achieved for the NV center [320], and even employed to demonstrate spin–photon entanglement at 1588 nm [322]. A final challenge is scaling up: while initial quantum repeater demonstrations could be achieved with single cavity-coupled defects (with a few auxiliary nuclear spin qubits), more advanced applications—for example, those employing error correction—will likely require an increased number of qubits per node. While some on-chip integration may be possible for arrays of open microcavities [222,262], nanofabricated approaches offer a clear opportunity to combine cavity-coupled qubits with integrated photonics routing structures [274,317,323] for large-scale on-chip applications [119–121].

In conclusion, while challenges still lie ahead, recent advances in cavity coupling of diamond defects have demonstrated the feasibility of realizing a coherent interface between single photons and long-lived solid-state spins. Such a platform places the field on the cusp of finally realizing many of the ideas that first inspired interest in diamond defects, and it may someday form the fundamental building block for practical quantum network applications.

Funding. National Defense Science and Engineering Graduate Fellowship; Canadian Institute for Advanced Research (Quantum Information Science Program); Canada Research Chairs (229003, 231949); Natural Sciences and Engineering Research Council of Canada (RGPIN 2020-04095, RGPIN 435554-13, RTI-2016-00089); Canada Foundation for Innovation (229003, 33488); Fonds de recherche du Québec–Nature et technologies (PR-253399); Institut Transdisciplinaire d'Information Quantique.

Acknowledgment. The authors thank Yannik Fontana for providing the defect diagrams used in Fig. 2, Christian Nguyen for providing the SiV spectrum used in Fig. 2, Bartholomeus Machielse for giving comments and providing the false-color SEM in Fig. 5, and Paul Barclay, Stefan Bogdanovic, and Daniel Riedel for providing insightful commentary on the paper.

Disclosures. The authors declare no conflicts of interest.

[†]These authors contributed equally to this work.

REFERENCES

1. N. Gisin, G. G. Ribordy, W. Tittel, and H. Zbinden, "Quantum cryptography," Rev. Mod. Phys. **74**, 145–195 (2002).
2. V. Scarani, H. Bechmann-Pasquinucci, N. J. Cerf, M. Dusek, N. Luetkenhaus, and M. Peev, "The security of practical quantum key distribution," Rev. Mod. Phys. **81**, 1301–1350 (2009).
3. H.-K. Lo, M. Curty, and K. Tamaki, "Secure quantum key distribution," Nat. Photonics **8**, 595–604 (2014).
4. S. Pirandola, U. L. Andersen, L. Banchi, M. Berta, D. Bunandar, R. Colbeck, D. Englund, T. Gehring, C. Lupo, C. Ottaviani, J. Pereira, M. Razavi, J. S. Shaari, M. Tomamichel, V. C. Usenko, G. Vallone, P. Villoresi, and P. Wallden, "Advances in quantum cryptography," Adv. Opt. Photon. **12**, 1012–1236 (2020).
5. T. D. Ladd, F. Jelezko, R. Laflamme, Y. Nakamura, C. Monroe, and J. L. O'Brien, "Quantum computers," Nature **464**, 45–53 (2010).
6. C. Degen, F. Reinhard, and P. Cappellaro, "Quantum sensing," Rev. Mod. Phys. **89**, 035002 (2017).
7. H. J. Kimble, "The quantum internet," Nature **453**, 1023–1030 (2008).
8. S. Wehner, D. Elkouss, and R. Hanson, "Quantum internet: a vision for the road ahead," Science **362**, eaam9288 (2018).
9. C. Monroe, R. Raussendorf, A. Ruthven, K. R. Brown, P. Maunz, L.-M. Duan, and J. Kim, "Large-scale modular quantum-computer architecture with atomic memory and photonic interconnects," Phys. Rev. A **89**, 022317 (2014).
10. K. Nemoto, M. Trupke, S. Devitt, A. M. Stephens, B. Scharfenberger, K. Buczak, T. Nöbauer, M. S. Everitt, J. Schmiedmayer, and W. J. Munro, "Photonic architecture for scalable quantum information processing in diamond," Phys. Rev. X **4**, 031022 (2014).
11. J. F. Fitzsimons, "Private quantum computation: an introduction to blind quantum computing and related protocols," npj Quantum Inf. **3**, 23 (2017).
12. R. Jozsa, D. S. Abrams, J. P. Dowling, and C. P. Williams, "Quantum clock synchronization based on shared prior entanglement," Phys. Rev. Lett. **85**, 2010–2013 (2000).
13. V. Giovannetti, S. Lloyd, and L. Maccone, "Quantum-enhanced positioning and clock synchronization," Nature **412**, 417–419 (2001).
14. P. Kómár, E. M. Kessler, M. Bishof, L. Jiang, A. S. Sørensen, J. Ye, and M. D. Lukin, "A quantum network of clocks," Nat. Phys. **10**, 582–587 (2014).
15. D. Gottesman, T. Jennewein, and S. Croke, "Longer-baseline telescopes using quantum repeaters," Phys. Rev. Lett. **109**, 070503 (2012).
16. E. Khabiboulline, J. Borregaard, K. De Greve, and M. Lukin, "Optical interferometry with quantum networks," Phys. Rev. Lett. **123**, 070504 (2019).
17. H.-J. Briegel, W. Dür, J. I. Cirac, and P. Zoller, "Quantum repeaters: the role of imperfect local operations in quantum communication," Phys. Rev. Lett. **81**, 5932–5935 (1998).
18. W. J. Munro, K. Azuma, K. Tamaki, and K. Nemoto, "Inside quantum repeaters," IEEE J. Sel. Top. Quantum Electron. **21**, 78–90 (2015).
19. S. Muralidharan, L. Li, J. Kim, N. Lütkenhaus, M. D. Lukin, and L. Jiang, "Optimal architectures for long distance quantum communication," Sci. Rep. **6**, 20463 (2016).
20. P. Goy, J. M. Raimond, M. Gross, and S. Haroche, "Observation of cavity-enhanced single-atom spontaneous emission," Phys. Rev. Lett. **50**, 1903–1906 (1983).

21. H. J. Kimble, "Strong interactions of single atoms and photons in cavity QED," Phys. Scr. **T76**, 127–137 (1998).
22. H. Mabuchi and A. C. Doherty, "Cavity quantum electrodynamics: coherence in context," Science **298**, 1372–1377 (2002).
23. K. J. Vahala, "Optical microcavities," Nature **424**, 839–846 (2003).
24. P. Lodahl, S. Mahmoodian, and S. Stobbe, "Interfacing single photons and single quantum dots with photonic nanostructures," Rev. Mod. Phys. **87**, 347–400 (2015).
25. A. Reiserer and G. Rempe, "Cavity-based quantum networks with single atoms and optical photons," Rev. Mod. Phys. **87**, 1379 (2015).
26. T. Pellizzari, S. A. Gardiner, J. I. Cirac, and P. Zoller, "Decoherence, continuous observation, and quantum computing: a cavity QED model," Phys. Rev. Lett. **75**, 3788–3791 (1995).
27. J. I. Cirac, P. Zoller, H. J. Kimble, and H. Mabuchi, "Quantum state transfer and entanglement distribution among distant nodes in a quantum network," Phys. Rev. Lett. **78**, 3221–3224 (1997).
28. T. E. Northup and R. Blatt, "Quantum information transfer using photons," Nat. Photonics **8**, 356–363 (2014).
29. J. McKeever, A. Boca, A. D. Boozer, R. Miller, J. R. Buck, A. Kuzmich, and H. J. Kimble, "Deterministic generation of single photons from one atom trapped in a cavity," Science **303**, 1992–1994 (2004).
30. P. Senellart, G. Solomon, and A. White, "High-performance semiconductor quantum-dot single-photon sources," Nat. Nanotechnol. **12**, 1026–1039 (2017).
31. E. Knill, R. Laflamme, and G. J. Milburn, "A scheme for efficient quantum computation with linear optics," Nature **409**, 46–52 (2001).
32. P. Kok, W. J. Munro, K. Nemoto, T. C. Ralph, J. P. Dowling, and G. J. Milburn, "Linear optical quantum computing with photonic qubits," Rev. Mod. Phys. **79**, 135–174 (2007).
33. B. Dayan, A. S. Parkins, T. Aoki, E. P. Ostby, K. J. Vahala, and H. J. Kimble, "A photon turnstile dynamically regulated by one atom," Science **319**, 1062–1065 (2008).
34. H. P. Specht, C. Nolleke, A. Reiserer, M. Uphoff, E. Figueroa, S. Ritter, and G. Rempe, "A single-atom quantum memory," Nature **473**, 190–193 (2011).
35. C. Clausen, I. Usmani, F. Bussières, N. Sangouard, M. Afzelius, H. de Riedmatten, and N. Gisin, "Quantum storage of photonic entanglement in a crystal," Nature **469**, 508–511 (2011).
36. Y.-H. Chen, M.-J. Lee, I.-C. Wang, S. Du, Y.-F. Chen, Y.-C. Chen, and I. A. Yu, "Coherent optical memory with high storage efficiency and large fractional delay," Phys. Rev. Lett. **110**, 083601 (2013).
37. A. Seri, A. Lenhard, D. Rieländer, M. Gündoğan, P. M. Ledingham, M. Mazzera, and H. de Riedmatten, "Quantum correlations between single telecom photons and a multimode on-demand solid-state quantum memory," Phys. Rev. X **7**, 021028 (2017).
38. B. B. Blinov, D. L. Moehring, L.-M. Duan, and C. Monroe, "Observation of entanglement between a single trapped atom and a single photon," Nature **428**, 153–157 (2004).
39. D. N. Matsukevich, T. Chanelière, M. Bhattacharya, S.-Y. Lan, S. D. Jenkins, T. A. B. Kennedy, and A. Kuzmich, "Entanglement of a photon and a collective atomic excitation," Phys. Rev. Lett. **95**, 040405 (2005).
40. J. Volz, M. Weber, D. Schlenk, W. Rosenfeld, J. Vrana, K. Saucke, C. Kurtsiefer, and H. Weinfurter, "Observation of entanglement of a single photon with a trapped atom," Phys. Rev. Lett. **96**, 030404 (2006).
41. E. Togan, Y. Chu, A. S. Trifonov, L. Jiang, J. Maze, L. Childress, M. V. G. Dutt, A. S. Sørensen, P. R. Hemmer, A. S. Zibrov, and M. D. Lukin, "Quantum entanglement between an optical photon and a solid-state spin qubit," Nature **466**, 730–734 (2010).
42. W. B. Gao, P. Fallahi, E. Togan, J. Miguel-Sanchez, and A. Imamoglu, "Observation of entanglement between a quantum dot spin and a single photon," Nature **491**, 426–430 (2012).
43. K. De Greve, L. Yu, P. L. McMahon, J. S. Pelc, C. M. Natarajan, N. Y. Kim, E. Abe, S. Maier, C. Schneider, M. Kamp, S. Höfling, R. H. Hadfield, A. Forchel, M. M. Fejer, and Y. Yamamoto, "Quantum-dot spin–photon entanglement via frequency downconversion to telecom wavelength," Nature **491**, 421–425 (2012).
44. T. Tiecke, J. Thompson, N. de Leon, L. Liu, V. Vuletic, and M. Lukin, "Nanophotonic quantum phase switch with a single atom," Nature **508**, 241–244 (2014).
45. S. Sun, H. Kim, G. S. Solomon, and E. Waks, "A quantum phase switch between a single solid-state spin and a photon," Nat. Nanotechnol. **11**, 539–544 (2016).
46. L.-M. Duan and H. J. Kimble, "Scalable photonic quantum computation through cavity-assisted interactions," Phys. Rev. Lett. **92**, 127902 (2004).
47. K. M. Beck, M. Hosseini, Y. Duan, and V. Vuletic, "Large conditional single-photon cross-phase modulation," Proc. Natl. Acad. Sci. USA **113**, 9740–9744 (2016).
48. B. Hacker, S. Welte, G. Rempe, and S. Ritter, "A photon–photon quantum gate based on a single atom in an optical resonator," Nature **536**, 193–196 (2016).
49. N. Sangouard, C. Simon, H. de Riedmatten, and N. Gisin, "Quantum repeaters based on atomic ensembles and linear optics," Rev. Mod. Phys. **83**, 33–80 (2011).
50. H. de Riedmatten and M. Afzelius, "Quantum light storage in solid state atomic ensembles," in *Engineering the Atom-Photon Interaction: Controlling Fundamental Processes with Photons, Atoms and Solids* (Springer, 2015), pp. 241–273.
51. C. H. Bennett, G. Brassard, S. Popescu, B. Schumacher, J. A. Smolin, and W. K. Wootters, "Purification of noisy entanglement and faithful teleportation via noisy channels," Phys. Rev. Lett. **76**, 722–725 (1996).
52. R. Reichle, D. Leibfried, E. Knill, J. Britton, R. B. Blakestad, J. D. Jost, C. Langer, R. Ozeri, S. Seidelin, and D. J. Wineland, "Experimental purification of two-atom entanglement," Nature **443**, 838–841 (2006).
53. N. Kalb, A. A. Reiserer, P. C. Humphreys, J. J. W. Bakermans, S. J. Kamerling, N. H. Nickerson, S. C. Benjamin, D. J. Twitchen, M. Markham, and R. Hanson, "Entanglement distillation between solid-state quantum network nodes," Science **356**, 928–932 (2017).
54. C. H. Bennett, G. Brassard, C. Crépeau, R. Jozsa, A. Peres, and W. K. Wootters, "Teleporting an unknown quantum state via dual classical and Einstein–Podolsky–Rosen channels," Phys. Rev. Lett. **70**, 1895–1899 (1993).
55. D. Bouwmeester, J.-W. Pan, K. Mattle, M. Eibl, H. Weinfurter, and A. Zeilinger, "Experimental quantum teleportation," Nature **390**, 575–579 (1997).
56. A. K. Ekert, "Quantum cryptography based on Bell's theorem," Phys. Rev. Lett. **67**, 661–663 (1991).
57. C. Cabrillo, J. I. Cirac, P. García-Fernández, and P. Zoller, "Creation of entangled states of distant atoms by interference," Phys. Rev. A **59**, 1025–1033 (1999).
58. S. D. Barrett and P. Kok, "Efficient high-fidelity quantum computation using matter qubits and linear optics," Phys. Rev. A **71**, 060310 (2005).
59. C.-W. Chou, J. Laurat, H. Deng, K. S. Choi, H. D. Riedmatten, D. Felinto, and H. J. Kimble, "Functional quantum nodes for entanglement distribution over scalable quantum networks," Science **316**, 1316–1320 (2007).
60. D. L. Moehring, P. Maunz, S. Olmschenk, K. C. Younge, D. N. Matsukevich, L.-M. Duan, and C. Monroe, "Entanglement of single-atom quantum bits at a distance," Nature **449**, 68–71 (2007).
61. J. Hofmann, M. Krug, N. Ortegel, L. Gérard, M. Weber, W. Rosenfeld, and H. Weinfurter, "Heralded entanglement between widely separated atoms," Science **337**, 72–75 (2012).
62. H. Bernien, B. Hensen, W. Pfaff, G. Koolstra, M. S. Blok, L. Robledo, T. H. Taminiau, M. Markham, D. J. Twitchen, L. Childress, and R. Hanson, "Heralded entanglement between solid-state qubits separated by three metres," Nature **497**, 86–90 (2013).
63. A. Delteil, Z. Sun, W.-B. Gao, E. Togan, S. Faelt, and A. Imamoğlu, "Generation of heralded entanglement between distant hole spins," Nat. Phys. **12**, 218–223 (2016).
64. R. Stockill, M. Stanley, L. Huthmacher, E. Clarke, M. Hugues, A. Miller, C. Matthiesen, C. Le Gall, and M. Atatüre, "Phase-tuned entangled state generation between distant spin qubits," Phys. Rev. Lett. **119**, 010503 (2017).
65. E. Purcell, "Spontaneous emission probabilities at radio frequencies," Phys. Rev. **69**, 681 (1946).
66. C. J. Axline, L. D. Burkhart, W. Pfaff, M. Zhang, K. Chou, P. Campagne-Ibarcq, P. Reinhold, L. Frunzio, S. M. Girvin, L. Jiang, M. H. Devoret, and R. J. Schoelkopf, "On-demand quantum state transfer and entanglement between remote microwave cavity memories," Nat. Phys. **14**, 705–710 (2018).
67. M. Varnava, D. E. Browne, and T. Rudolph, "Loss tolerance in one-way quantum computation via counterfactual error correction," Phys. Rev. Lett. **97**, 120501 (2006).
68. A. G. Fowler, D. S. Wang, C. D. Hill, T. D. Ladd, R. Van Meter, and L. C. L. Hollenberg, "Surface code quantum communication," Phys. Rev. Lett. **104**, 180503 (2010).

69. S. Muralidharan, J. Kim, N. Lütkenhaus, M. D. Lukin, and L. Jiang, "Ultrafast and fault-tolerant quantum communication across long distances," Phys. Rev. Lett. **112**, 250501 (2014).
70. W. J. Munro, A. M. Stephens, S. J. Devitt, K. A. Harrison, and K. Nemoto, "Quantum communication without the necessity of quantum memories," Nat. Photonics **6**, 777–781 (2012).
71. K. Azuma, K. Tamaki, and H.-K. Lo, "All-photonic quantum repeaters," Nat. Commun. **6**, 6787 (2015).
72. M. Pant, H. Krovi, D. Englund, and S. Guha, "Rate-distance tradeoff and resource costs for all-optical quantum repeaters," Phys. Rev. A **95**, 012304 (2017).
73. C. Schön, E. Solano, F. Verstraete, J. I. Cirac, and M. M. Wolf, "Sequential generation of entangled multiqubit states," Phys. Rev. Lett. **95**, 110503 (2005).
74. N. H. Lindner and T. Rudolph, "Proposal for pulsed on-demand sources of photonic cluster state strings," Phys. Rev. Lett. **103**, 113602 (2009).
75. I. Schwartz, D. Cogan, E. R. Schmidgall, Y. Don, L. Gantz, O. Kenneth, N. H. Lindner, and D. Gershoni, "Deterministic generation of a cluster state of entangled photons," Science **354**, 434–437 (2016).
76. D. Buterakos, E. Barnes, and S. E. Economou, "Deterministic generation of all-photonic quantum repeaters from solid-state emitters," Phys. Rev. X **7**, 041023 (2017).
77. J. Borregaard, H. Pichler, T. Schröder, M. D. Lukin, P. Lodahl, and A. S. Sørensen, "One-way quantum repeater based on near-deterministic photon-emitter interfaces," Phys. Rev. X **10**, 021071 (2020).
78. J. Borregaard, A. S. Sørensen, and P. Lodahl, "Quantum networks with deterministic spin–photon interfaces," Adv. Quantum Technol. **2**, 1800091 (2019).
79. P. Lodahl, "Quantum-dot based photonic quantum networks," Quantum Sci. Technol. **3**, 013001 (2017).
80. D. Wang, H. Kelkar, D. Martin-Cano, D. Rattenbacher, A. Shkarin, T. Utikal, S. Götzinger, and V. Sandoghdar, "Turning a molecule into a coherent two-level quantum system," Nat. Phys. **15**, 483–489 (2019).
81. H. Takahashi, E. Kassa, C. Christoforou, and M. Keller, "Strong coupling of a single ion to an optical cavity," Phys. Rev. Lett. **124**, 013602 (2020).
82. P. Kobel, M. Breyer, and M. Köhl, "Deterministic spin-photon entanglement from a trapped ion in a fiber Fabry–Perot cavity," arXiv:2005.09124 (2020).
83. D. D. Awschalom, R. Hanson, J. Wrachtrup, and B. B. Zhou, "Quantum technologies with optically interfaced solid-state spins," Nat. Photonics **12**, 516 (2018).
84. M. Atatüre, D. Englund, N. Vamivakas, S.-Y. Lee, and J. Wrachtrup, "Material platforms for spin-based photonic quantum technologies," Nat. Rev. Mater. **3**, 38–51 (2018).
85. T. Schröder, S. L. Mouradian, J. Zheng, M. E. Trusheim, M. Walsh, E. H. Chen, L. Li, I. Bayn, and D. Englund, "Quantum nanophotonics in diamond," J. Opt. Soc. Am. B **33**, B65–B83 (2016).
86. S. Johnson, P. R. Dolan, and J. M. Smith, "Diamond photonics for distributed quantum networks," Prog. Quantum Electron. **55**, 129–165 (2017).
87. C. Bradac, W. Gao, J. Forneris, M. E. Trusheim, and I. Aharonovich, "Quantum nanophotonics with group IV defects in diamond," Nat. Commun. **10**, 5625 (2019).
88. T. Zhong, J. M. Kindem, J. G. Bartholomew, J. Rochman, I. Craiciu, V. Verma, S. W. Nam, F. Marsili, M. D. Shaw, A. D. Beyer, and A. Faraon, "Optically addressing single rare-earth ions in a nanophotonic cavity," Phys. Rev. Lett. **121**, 183603 (2018).
89. A. Dibos, M. Raha, C. Phenicie, and J. Thompson, "Atomic source of single photons in the telecom band," Phys. Rev. Lett. **120**, 243601 (2018).
90. A. L. Crook, C. P. Anderson, K. C. Miao, A. Bourassa, H. Lee, S. L. Bayliss, D. O. Bracher, X. Zhang, H. Abe, T. Ohshima, E. L. Hu, and D. D. Awschalom, "Purcell enhancement of a single silicon carbide color center with coherent spin control," Nano Lett. **20**, 3427–3434 (2020).
91. L. C. Bassett, A. Alkauskas, A. L. Exarhos, and K.-M. C. Fu, "Quantum defects by design," Nanophotonics **8**, 1867–1888 (2019).
92. A. M. Zaitsev, *Optical Properties of Diamond: A Data Handbook* (Springer, 2001).
93. C. Bradley, J. Randall, M. Abobeih, R. Berrevoets, M. Degen, M. Bakker, M. Markham, D. Twitchen, and T. Taminiau, "A ten-qubit solid-state spin register with quantum memory up to one minute," Phys. Rev. X **9**, 031045 (2019).
94. J. R. Maze, A. Gali, E. Togan, Y. Chu, A. Trifonov, E. Kaxiras, and M. D. Lukin, "Properties of nitrogen-vacancy centers in diamond: the group theoretic approach," New J. Phys. **13**, 025025 (2011).
95. M. W. Doherty, N. B. Manson, P. Delaney, and L. C. L. Hollenberg, "The negatively charged nitrogen-vacancy centre in diamond: the electronic solution," New J. Phys. **13**, 025019 (2011).
96. L. Childress, J. M. Taylor, A. S. Sørensen, and M. D. Lukin, "Fault-tolerant quantum communication based on solid-state photon emitters," Phys. Rev. Lett. **96**, 070504 (2006).
97. N. Lo Piparo, M. Razavi, and W. J. Munro, "Memory-assisted quantum key distribution with a single nitrogen-vacancy center," Phys. Rev. A **96**, 052313 (2017).
98. F. Rozpedek, R. Yehia, K. Goodenough, M. Ruf, P. C. Humphreys, R. Hanson, S. Wehner, and D. Elkouss, "Near-term quantum-repeater experiments with nitrogen-vacancy centers: overcoming the limitations of direct transmission," Phys. Rev. A **99**, 052330 (2019).
99. B. Hensen, H. Bernien, A. E. Dréau, A. Reiserer, N. Kalb, M. S. Blok, J. Ruitenberg, R. F. L. Vermeulen, R. N. Schouten, C. Abellán, W. Amaya, V. Pruneri, M. W. Mitchell, M. Markham, D. J. Twitchen, D. Elkouss, S. Wehner, T. H. Taminiau, and R. Hanson, "Loophole-free Bell inequality violation using electron spins separated by 1.3 kilometres," Nature **526**, 682–686 (2015).
100. W. Pfaff, B. J. Hensen, H. Bernien, S. B. V. Dam, M. S. Blok, T. H. Taminiau, M. J. Tiggelman, R. N. Schouten, M. Markham, D. J. Twitchen, and R. Hanson, "Unconditional quantum teleportation between distant solid-state quantum bits," Science **345**, 532–535 (2014).
101. P. C. Humphreys, N. Kalb, J. P. J. Morits, R. N. Schouten, R. F. L. Vermeulen, D. J. Twitchen, M. Markham, and R. Hanson, "Deterministic delivery of remote entanglement on a quantum network," Nature **558**, 268–273 (2018).
102. D. Sukachev, A. Sipahigil, C. Nguyen, M. Bhaskar, R. Evans, F. Jelezko, and M. Lukin, "Silicon-vacancy spin qubit in diamond: a quantum memory exceeding 10 ms with single-shot state readout," Phys. Rev. Lett. **119**, 223602 (2017).
103. B. C. Rose, D. Huang, Z.-H. Zhang, P. Stevenson, A. M. Tyryshkin, S. Sangtawesin, S. Srinivasan, L. Loudin, M. L. Markham, A. M. Edmonds, D. J. Twitchen, S. A. Lyon, and N. P. D. Leon, "Observation of an environmentally insensitive solid-state spin defect in diamond," Science **361**, 60–63 (2018).
104. M. H. Metsch, K. Senkalla, B. Tratzmiller, J. Scheuer, M. Kern, J. Achard, A. Tallaire, M. B. Plenio, P. Siyushev, and F. Jelezko, "Initialization and readout of nuclear spins via a negatively charged silicon-vacancy center in diamond," Phys. Rev. Lett. **122**, 190503 (2019).
105. A. Huck and U. L. Andersen, "Coupling single emitters to quantum plasmonic circuits," Nanophotonics **5**, 483–495 (2016).
106. M. Trupke, E. A. Hinds, S. Eriksson, E. A. Curtis, Z. Moktadir, E. Kukharenka, and M. Kraft, "Microfabricated high-finesse optical cavity with open access and small volume," Appl. Phys. Lett. **87**, 211106 (2005).
107. D. Hunger, T. Steinmetz, Y. Colombe, C. Deutsch, T. W. Hänsch, and J. Reichel, "A fiber Fabry–Perot cavity with high finesse," New J. Phys. **12**, 065038 (2010).
108. R. Albrecht, A. Bommer, C. Deutsch, J. Reichel, and C. Becher, "Coupling of a single nitrogen-vacancy center in diamond to a fiber-based microcavity," Phys. Rev. Lett. **110**, 243602 (2013).
109. R. Albrecht, A. Bommer, C. Pauly, F. Mücklich, A. W. Schell, P. Engel, T. Schröder, O. Benson, J. Reichel, and C. Becher, "Narrow-band single photon emission at room temperature based on a single nitrogen-vacancy center coupled to an all-fiber-cavity," Appl. Phys. Lett. **105**, 073113 (2014).
110. S. Johnson, P. R. Dolan, T. Grange, A. A. P. Trichet, G. Hornecker, Y. C. Chen, L. Weng, G. M. Hughes, A. A. R. Watt, A. Auffèves, and J. M. Smith, "Tunable cavity coupling of the zero phonon line of a nitrogen-vacancy defect in diamond," New J. Phys. **17**, 122003 (2015).
111. H. Kaupp, T. Huemmer, M. Mader, B. Schlederer, J. Benedikter, P. Haeusser, H.-C. Chang, H. Fedder, T. W. Haensch, and D. Hunger, "Purcell-enhanced single-photon emission from nitrogen-vacancy centers coupled to a tunable microcavity," Phys. Rev. Appl. **6**, 054010 (2016).

112. J. Benedikter, H. Kaupp, T. Huemmer, Y. Liang, A. Bommer, C. Becher, A. Krueger, J. M. Smith, T. W. Haensch, and D. Hunger, "Cavity-enhanced single-photon source based on the silicon-vacancy center in diamond," Phys. Rev. Appl. **7**, 024031 (2017).
113. E. Janitz, M. Ruf, M. Dimock, A. Bourassa, J. Sankey, and L. Childress, "Fabry-Perot microcavity for diamond-based photonics," Phys. Rev. A **92**, 043844 (2015).
114. M. Ruf, M. IJspeert, S. van Dam, N. de Jong, H. van den Berg, G. Evers, and R. Hanson, "Optically coherent nitrogen-vacancy centers in micrometer-thin etched diamond membranes," Nano Lett. **19**, 3987–3992 (2019).
115. T. M. Babinec, J. T. Choy, K. J. M. Smith, M. Khan, and M. Loncar, "Design and focused ion beam fabrication of single crystal diamond nanobeam cavities," J. Vac. Sci. Technol. B **29**, 010601 (2011).
116. A. Faraon, P. E. Barclay, C. Santori, K.-M. C. Fu, and R. G. Beausoleil, "Resonant enhancement of the zero-phonon emission from a colour centre in a diamond cavity," Nat. Photonics **5**, 301–305 (2011).
117. J. Wolters, A. W. Schell, G. Kewes, N. Nüsse, M. Schoengen, H. Döscher, T. Hannappel, B. Löchel, M. Barth, and O. Benson, "Enhancement of the zero phonon line emission from a single nitrogen vacancy center in a nanodiamond via coupling to a photonic crystal cavity," Appl. Phys. Lett. **97**, 141108 (2010).
118. P. E. Barclay, K.-M. C. Fu, C. Santori, A. Faraon, and R. G. Beausoleil, "Hybrid nanocavity resonant enhancement of color center emission in diamond," Phys. Rev. X **1**, 011007 (2011).
119. A. W. Elshaari, W. Pernice, K. Srinivasan, O. Benson, and V. Zwiller, "Hybrid integrated quantum photonic circuits," Nat. Photonics **14**, 285–298 (2020).
120. J.-H. Kim, S. Aghaeimeibodi, J. Carolan, D. Englund, and E. Waks, "Hybrid integration methods for on-chip quantum photonics," Optica **7**, 291–308 (2020).
121. N. H. Wan, T.-J. Lu, K. C. Chen, M. P. Walsh, M. E. Trusheim, L. De Santis, E. A. Bersin, I. B. Harris, S. L. Mouradian, I. R. Christen, E. S. Bielejec, and D. Englund, "Large-scale integration of artificial atoms in hybrid photonic circuits," Nature **583**, 226–231 (2020).
122. C. Nguyen, D. Sukachev, M. Bhaskar, B. Machielse, D. Levonian, E. Knall, P. Stroganov, R. Riedinger, H. Park, M. Lončar, and M. Lukin, "Quantum network nodes based on diamond qubits with an efficient nanophotonic interface," Phys. Rev. Lett. **123**, 183602 (2019).
123. C. T. Nguyen, D. D. Sukachev, M. K. Bhaskar, B. Machielse, D. S. Levonian, E. N. Knall, P. Stroganov, C. Chia, M. J. Burek, R. Riedinger, H. Park, M. Lončar, and M. D. Lukin, "An integrated nanophotonic quantum register based on silicon-vacancy spins in diamond," Phys. Rev. B **100**, 165428 (2019).
124. M. K. Bhaskar, R. Riedinger, B. Machielse, D. S. Levonian, C. T. Nguyen, E. N. Knall, H. Park, D. Englund, M. Lončar, D. D. Sukachev, and M. D. Lukin, "Experimental demonstration of memory-enhanced quantum communication," Nature **580**, 60–64 (2020).
125. M. Fox, *Quantum Optics: An Introduction* (Oxford University, 2006).
126. J. Vučković, "Quantum optics and cavity QED with quantum dots in photonic crystals," in *Quantum Optics and Nanophotonics* (Oxford University Press, 2017).
127. H. Kaupp, C. Deutsch, H.-C. Chang, J. Reichel, T. W. Hänsch, and D. Hunger, "Scaling laws of the cavity enhancement for nitrogen-vacancy centers in diamond," Phys. Rev. A **88**, 053812 (2013).
128. T. Grange, G. Hornecker, D. Hunger, J.-P. Poizat, J.-M. Gérard, P. Senellart, and A. Auffèves, "Cavity-funneled generation of indistinguishable single photons from strongly dissipative quantum emitters," Phys. Rev. Lett. **114**, 193601 (2015).
129. R. Høy Jensen, E. Janitz, Y. Fontana, Y. He, O. Gobron, I. P. Radko, M. Bhaskar, R. Evans, C. D. Rodríguez Rosenblueth, L. Childress, A. Huck, and U. Lund Andersen, "Cavity-enhanced photon emission from a single germanium-vacancy center in a diamond membrane," Phys. Rev. Appl. **13**, 064016 (2020).
130. T. Legero, T. Wilk, A. Kuhn, and G. Rempe, "Time-resolved two-photon quantum interference," Appl. Phys. B **77**, 797–802 (2003).
131. H. Bernien, L. Childress, L. Robledo, M. Markham, D. Twitchen, and R. Hanson, "Two-photon quantum interference from separate nitrogen vacancy centers in diamond," Phys. Rev. Lett. **108**, 043604 (2012).
132. M. W. Doherty, N. B. Manson, P. Delaney, F. Jelezko, J. Wrachtrup, and L. C. L. Hollenberg, "The nitrogen-vacancy colour centre in diamond," Phys. Rep. **528**, 1–45 (2013).
133. A. Gali, "Ab initio theory of the nitrogen-vacancy center in diamond," Nanophotonics **8**, 1907–1943 (2019).
134. T. Muller, C. Hepp, B. Pingault, E. Neu, S. Gsell, M. Schreck, H. Sternschulte, D. Steinmüller-Nethl, C. Becher, and M. Atatüre, "Optical signatures of silicon-vacancy spins in diamond," Nat. Commun. **5**, 3328 (2014).
135. C. Hepp, T. Müller, V. Waselowski, J. N. Becker, B. Pingault, H. Sternschulte, D. Steinmüller-Nethl, A. Gali, J. R. Maze, M. Atatüre, and C. Becher, "Electronic structure of the silicon vacancy color center in diamond," Phys. Rev. Lett. **112**, 036405 (2014).
136. P. Siyushev, M. H. Metsch, A. Ijaz, J. M. Binder, M. K. Bhaskar, D. D. Sukachev, A. Sipahigil, R. E. Evans, C. T. Nguyen, M. D. Lukin, P. R. Hemmer, Y. N. Palyanov, I. N. Kupriyanov, Y. M. Borzdov, L. J. Rogers, and F. Jelezko, "Optical and microwave control of germanium-vacancy center spins in diamond," Phys. Rev. B **96**, 081201 (2017).
137. A. E. Rugar, C. Dory, S. Sun, and J. Vučković, "Characterization of optical and spin properties of single tin-vacancy centers in diamond nanopillars," Phys. Rev. B **99**, 205417 (2019).
138. M. E. Trusheim, B. Pingault, N. H. Wan, M. Gündoğan, L. De Santis, R. Debroux, D. Gangloff, C. Purser, K. C. Chen, M. Walsh, J. J. Rose, J. N. Becker, B. Lienhard, E. Bersin, I. Paradeisanos, G. Wang, D. Lyzwa, A. R.-P. Montblanch, G. Malladi, H. Bakhru, A. C. Ferrari, I. A. Walmsley, M. Atatüre, and D. Englund, "Transform-limited photons from a coherent tin-vacancy spin in diamond," Phys. Rev. Lett. **124**, 023602 (2020).
139. R. N. Patel, T. Schröder, N. Wan, L. Li, S. L. Mouradian, E. H. Chen, and D. R. Englund, "Efficient photon coupling from a diamond nitrogen vacancy center by integration with silica fiber," Light Sci. Appl. **5**, e16032 (2016).
140. M. J. Burek, C. Meuwly, R. E. Evans, M. K. Bhaskar, A. Sipahigil, S. Meesala, B. Machielse, D. D. Sukachev, C. T. Nguyen, J. L. Pacheco, E. Bielejec, M. D. Lukin, and M. Loncar, "Fiber-coupled diamond quantum nanophotonic interface," Phys. Rev. Appl. **8**, 024026 (2017).
141. H. Tanji-Suzuki, I. D. Leroux, M. H. Schleier-Smith, M. Cetina, A. T. Grier, J. Simon, and V. Vuletić, "Chapter 4–Interaction between atomic ensembles and optical resonators: classical description," in *Advances in Atomic, Molecular, and Optical Physics* (Academic, 2011), Vol. **60**, pp. 201–237.
142. E. Waks and J. Vuckovic, "Dipole induced transparency in drop-filter cavity-waveguide Systems," Phys. Rev. Lett. **96**, 153601 (2006).
143. E. Waks and J. Vuckovic, "Dispersive properties and large Kerr nonlinearities using dipole-induced transparency in a single-sided cavity," Phys. Rev. A **73**, 041803 (2006).
144. A. Imamolu, D. D. Awschalom, G. Burkard, D. P. DiVincenzo, D. Loss, M. Sherwin, and A. Small, "Quantum information processing using quantum dot spins and cavity QED," Phys. Rev. Lett. **83**, 4204–4207 (1999).
145. L. Jiang, J. M. Taylor, K. Nemoto, W. J. Munro, R. Van Meter, and M. D. Lukin, "Quantum repeater with encoding," Phys. Rev. A **79**, 032325 (2009).
146. F. Jelezko and J. Wrachtrup, "Single defect centres in diamond: a review," Phys. Status Solidi A **203**, 3207–3225 (2006).
147. S. B. van Dam, M. Walsh, M. J. Degen, E. Bersin, S. L. Mouradian, A. Galiullin, M. Ruf, M. IJspeert, T. H. Taminiau, R. Hanson, and D. R. Englund, "Optical coherence of diamond nitrogen-vacancy centers formed by ion implantation and annealing," Phys. Rev. B **99**, 161203 (2019).
148. M. H. Abobeih, J. Cramer, M. A. Bakker, N. Kalb, M. Markham, D. J. Twitchen, and T. H. Taminiau, "One-second coherence for a single electron spin coupled to a multi-qubit nuclear-spin environment," Nat. Commun. **9**, 2552 (2018).
149. R. E. Evans, A. Sipahigil, D. D. Sukachev, A. S. Zibrov, and M. D. Lukin, "Narrow-linewidth homogeneous optical emitters in diamond nanostructures via silicon ion implantation," Phys. Rev. Appl. **5**, 044010 (2016).
150. J. P. Goss, P. R. Briddon, M. J. Rayson, S. J. Sque, and R. Jones, "Vacancy-impurity complexes and limitations for implantation doping of diamond," Phys. Rev. B **72**, 035214 (2005).
151. J. M. Smith, S. A. Meynell, A. C. B. Jayich, and J. Meijer, "Colour centre generation in diamond for quantum technologies," Nanophotonics **8**, 1889–1906 (2019).
152. J. R. Rabeau, P. Reichart, G. Tamanyan, D. N. Jamieson, S. Prawer, F. Jelezko, T. Gaebel, I. Popa, M. Domhan, and J. Wrachtrup, "Implantation of labelled single nitrogen vacancy centers in diamond using N-15," Appl. Phys. Lett. **88**, 023113 (2006).

153. S. Pezzagna, B. Naydenov, F. Jelezko, J. Wrachtrup, and J. Meijer, "Creation efficiency of nitrogen-vacancy centres in diamond," New J. Phys. **12**, 065017 (2010).
154. J. O. Orwa, C. Santori, K. M. C. Fu, B. Gibson, D. Simpson, I. Aharonovich, A. Stacey, A. Cimmino, P. Balog, M. Markham, D. Twitchen, A. D. Greentree, R. G. Beausoleil, and S. Prawer, "Engineering of nitrogen-vacancy color centers in high purity diamond by ion implantation and annealing," J. Appl. Phys. **109**, 083530 (2011).
155. J. F. Ziegler and J. P. Biersack, "The stopping and range of ions in matter," in *Treatise on Heavy-Ion Science*, Vol. **6**, Astrophysics, Chemistry, and Condensed Matter (Springer, 1985), pp. 93–129.
156. J. Meijer, B. Burchard, M. Domhan, C. Wittmann, T. Gaebel, I. Popa, F. Jelezko, and J. Wrachtrup, "Generation of single color centers by focused nitrogen implantation," Appl. Phys. Lett. **87**, 261909 (2005).
157. M. Lesik, P. Spinicelli, S. Pezzagna, P. Happel, V. Jacques, O. Salord, B. Rasser, A. Delobbe, P. Sudraud, A. Tallaire, J. Meijer, and J.-F. Roch, "Maskless and targeted creation of arrays of colour centres in diamond using focused ion beam technology," Phys. Status Solidi A **210**, 2055–2059 (2013).
158. S. Tamura, G. Koike, A. Komatsubara, T. Teraji, S. Onoda, L. P. McGuinness, L. Rogers, B. Naydenov, E. Wu, L. Yan, F. Jelezko, T. Ohshima, J. Isoya, T. Shinada, and T. Tanii, "Array of bright silicon-vacancy centers in diamond fabricated by low-energy focused ion beam implantation," Appl. Phys. Express **7**, 115201 (2014).
159. T. Schröder, M. E. Trusheim, M. Walsh, L. Li, J. Zheng, M. Schukraft, A. Sipahigil, R. E. Evans, D. D. Sukachev, C. T. Nguyen, J. L. Pacheco, R. M. Camacho, E. S. Bielejec, M. D. Lukin, and D. Englund, "Scalable focused ion beam creation of nearly lifetime-limited single quantum emitters in diamond nanostructures," Nat. Commun. **8**, 15376 (2017).
160. D. M. Toyli, C. D. Weis, G. D. Fuchs, T. Schenkel, and D. D. Awschalom, "Chip-scale nanofabrication of single spins and spin arrays in diamond," Nano Lett. **10**, 3168–3172 (2010).
161. P. Spinicelli, A. Dréau, L. Rondin, F. Silva, J. Achard, S. Xavier, S. Bansropun, T. Debuisschert, S. Pezzagna, J. Meijer, V. Jacques, and J.-F. Roch, "Engineered arrays of nitrogen-vacancy color centers in diamond based on implantation of CN-molecules through nanoapertures," New J. Phys. **13**, 025014 (2011).
162. I. Bayn, E. H. Chen, M. E. Trusheim, L. Li, T. Schröder, O. Gaathon, M. Lu, A. Stein, M. Liu, K. Kisslinger, H. Clevenson, and D. Englund, "Generation of ensembles of individually resolvable nitrogen vacancies using nanometer-scale apertures in ultrahigh-aspect ratio planar implantation masks," Nano Lett. **15**, 1751–1758 (2015).
163. D. Scarabelli, M. Trusheim, O. Gaathon, D. Englund, and S. J. Wind, "Nanoscale engineering of closely-spaced electronic spins in diamond," Nano Lett. **16**, 4982–4990 (2016).
164. A. E. Rugar, H. Lu, C. Dory, S. Sun, P. J. McQuade, Z.-X. Shen, N. A. Melosh, and J. Vučković, "Generation of tin-vacancy centers in diamond via shallow ion implantation and subsequent diamond overgrowth," Nano Lett. **20**, 1614–1619 (2020).
165. B. Naydenov, F. Reinhard, A. Lämmle, V. Richter, R. Kalish, U. F. S. D'Haenens-Johansson, M. Newton, F. Jelezko, and J. Wrachtrup, "Increasing the coherence time of single electron spins in diamond by high temperature annealing," Appl. Phys. Lett. **97**, 242511 (2010).
166. Y. Chu, N. de Leon, B. Shields, B. Hausmann, R. Evans, E. Togan, M. J. Burek, M. Markham, A. Stacey, A. Zibrov, A. Yacoby, D. Twitchen, M. Loncar, H. Park, P. Maletinsky, and M. Lukin, "Coherent optical transitions in implanted nitrogen vacancy centers," Nano Lett. **14**, 1982–1986 (2014).
167. T. Iwasaki, Y. Miyamoto, T. Taniguchi, P. Siyushev, M. H. Metsch, F. Jelezko, and M. Hatano, "Tin-vacancy quantum emitters in diamond," Phys. Rev. Lett. **119**, 253601 (2017).
168. J. Lang, S. Häußler, J. Fuhrmann, R. Waltrich, S. Laddha, J. Scharpf, A. Kubanek, B. Naydenov, and F. Jelezko, "Long optical coherence times of shallow-implanted, negatively charged silicon vacancy centers in diamond," Appl. Phys. Lett. **116**, 064001 (2020).
169. Y. N. Palyanov, I. N. Kupriyanov, Y. M. Borzdov, and N. V. Surovtsev, "Germanium: a new catalyst for diamond synthesis and a new optically active impurity in diamond," Sci. Rep. **5**, 14789 (2015).
170. Y. N. Palyanov, I. N. Kupriyanov, Y. M. Borzdov, A. F. Khokhryakov, and N. V. Surovtsev, "High-pressure synthesis and characterization of Ge-doped single crystal diamond," Cryst. Growth Des. **16**, 3510–3518 (2016).
171. Y. N. Palyanov, I. N. Kupriyanov, and Y. M. Borzdov, "High-pressure synthesis and characterization of Sn-doped single crystal diamond," Carbon **143**, 769–775 (2019).
172. L. J. Rogers, K. D. Jahnke, T. Teraji, L. Marseglia, C. Müller, B. Naydenov, H. Schauffert, C. Kranz, J. Isoya, L. P. McGuinness, and F. Jelezko, "Multiple intrinsically identical single-photon emitters in the solid state," Nat. Commun. **5**, 4739 (2014).
173. K. Bray, B. Regan, A. Trycz, R. Previdi, G. Seniutinas, K. Ganesan, M. Kianinia, S. Kim, and I. Aharonovich, "Single crystal diamond membranes and photonic resonators containing germanium vacancy color centers," ACS Photon. **5**, 4817–4822 (2018).
174. K. Ohno, F. Joseph Heremans, L. C. Bassett, B. A. Myers, D. M. Toyli, A. C. Bleszynski Jayich, C. J. Palmstrøm, and D. D. Awschalom, "Engineering shallow spins in diamond with nitrogen delta-doping," Appl. Phys. Lett. **101**, 082413 (2012).
175. J. C. Lee, D. O. Bracher, S. Cui, K. Ohno, C. A. McLellan, X. Zhang, P. Andrich, B. Alemán, K. J. Russell, A. P. Magyar, I. Aharonovich, A. Bleszynski Jayich, D. Awschalom, and E. L. Hu, "Deterministic coupling of delta-doped nitrogen vacancy centers to a nanobeam photonic crystal cavity," Appl. Phys. Lett. **105**, 261101 (2014).
176. J. Martin, R. Wannemacher, J. Teichert, L. Bischoff, and B. Köhler, "Generation and detection of fluorescent color centers in diamond with submicron resolution," Appl. Phys. Lett. **75**, 3096–3098 (1999).
177. B. Campbell and A. Mainwood, "Radiation damage of diamond by electron and gamma irradiation," Phys. Status Solidi A **181**, 99–107 (2000).
178. C. A. McLellan, B. A. Myers, S. Kraemer, K. Ohno, D. D. Awschalom, and A. C. Bleszynski Jayich, "Patterned formation of highly coherent nitrogen-vacancy centers using a focused electron irradiation technique," Nano Lett. **16**, 2450–2454 (2016).
179. Y.-C. Chen, P. S. Salter, S. Knauer, L. Weng, A. C. Frangeskou, C. J. Stephen, S. N. Ishmael, P. R. Dolan, S. Johnson, B. L. Green, G. W. Morley, M. E. Newton, J. G. Rarity, M. J. Booth, and J. M. Smith, "Laser writing of coherent colour centres in diamond," Nat. Photonics **11**, 77–80 (2017).
180. K. D. Jahnke, A. Sipahigil, J. M. Binder, M. W. Doherty, M. Metsch, L. J. Rogers, N. B. Manson, M. D. Lukin, and F. Jelezko, "Electron–phonon processes of the silicon-vacancy centre in diamond," New J. Phys. **17**, 043011 (2015).
181. K.-M. C. Fu, C. Santori, P. E. Barclay, L. J. Rogers, N. B. Manson, and R. G. Beausoleil, "Observation of the dynamic Jahn-Teller effect in the excited states of nitrogen-vacancy centers in diamond," Phys. Rev. Lett. **103**, 256404 (2009).
182. A. Gali and J. R. Maze, "Ab initio study of the split silicon-vacancy defect in diamond: electronic structure and related properties," Phys. Rev. B **88**, 235205 (2013).
183. A. Sipahigil, "Quantum optics with diamond color centers coupled to nanophotonic devices," Ph.D. thesis (Harvard University, 2017).
184. L. Robledo, H. Bernien, I. van Weperen, and R. Hanson, "Control and coherence of the optical transition of single nitrogen vacancy centers in diamond," Phys. Rev. Lett. **105**, 177403 (2010).
185. A. Dietrich, K. D. Jahnke, J. M. Binder, T. Teraji, J. Isoya, L. J. Rogers, and F. Jelezko, "Isotopically varying spectral features of silicon-vacancy in diamond," New J. Phys. **16**, 113019 (2014).
186. M. Bhaskar, D. Sukachev, A. Sipahigil, R. Evans, M. Burek, C. Nguyen, L. Rogers, P. Siyushev, M. Metsch, H. Park, F. Jelezko, M. Lončar, and M. Lukin, "Quantum nonlinear optics with a germanium-vacancy color center in a nanoscale diamond waveguide," Phys. Rev. Lett. **118**, 223603 (2017).
187. J. Görlitz, D. Herrmann, G. Thiering, P. Fuchs, M. Gandil, T. Iwasaki, T. Taniguchi, M. Kieschnick, J. Meijer, M. Hatano, A. Gali, and C. Becher, "Spectroscopic investigations of negatively charged tin-vacancy centres in diamond," New J. Phys. **22**, 013048 (2020).
188. M. E. Trusheim, N. H. Wan, K. C. Chen, C. J. Ciccarino, J. Flick, R. Sundararaman, G. Malladi, E. Bersin, M. Walsh, B. Lienhard, H. Bakhru, P. Narang, and D. Englund, "Lead-related quantum emitters in diamond," Phys. Rev. B **99**, 075430 (2019).
189. S. D. Tchernij, T. Luehmann, T. Herzig, J. Kuepper, A. Damin, S. Santonocito, M. Signorile, P. Traina, E. Moreva, F. Celegato, S. Pezzagna, I. P. Degiovanni, P. Olivero, M. Jaksic, J. Meijer, P. M. Genovese, and J. Forneris, "Single-photon emitters in lead-implanted single-crystal diamond," ACS Photon. **5**, 4864–4871 (2018).
190. D. M. Toyli, D. J. Christle, A. Alkauskas, B. B. Buckley, C. G. Van de Walle, and D. D. Awschalom, "Measurement and control of single

nitrogen-vacancy center spins above 600 K," Phys. Rev. X **2**, 031001 (2012).
191. B. C. Buchler, T. Kalkbrenner, C. Hettich, and V. Sandoghdar, "Measuring the quantum efficiency of the optical emission of single radiating dipoles using a scanning mirror," Phys. Rev. Lett. **95**, 063003 (2005).
192. I. P. Radko, M. Boll, N. M. Israelsen, N. Raatz, J. Meijer, F. Jelezko, U. L. Andersen, and A. Huck, "Determining the internal quantum efficiency of shallow-implanted nitrogen-vacancy defects in bulk diamond," Opt. Express **24**, 27715–27725 (2016).
193. A. Sipahigil, R. E. Evans, D. D. Sukachev, M. J. Burek, J. Borregaard, M. K. Bhaskar, C. T. Nguyen, J. L. Pacheco, H. A. Atikian, C. Meuwly, R. M. Camacho, F. Jelezko, E. Bielejec, H. Park, M. Loncar, and M. D. Lukin, "An integrated diamond nanophotonics platform for quantum-optical networks," Science **354**, 847–850 (2016).
194. D. Chen, Z. Mu, Y. Zhou, J. E. Fröch, A. Rasmit, C. Diederichs, N. Zheludev, I. Aharonovich, and W.-B. Gao, "Optical gating of resonance fluorescence from a single germanium vacancy color center in diamond," Phys. Rev. Lett. **123**, 033602 (2019).
195. C. Santori, P. E. Barclay, K.-M. C. Fu, R. G. Beausoleil, S. Spillane, and M. Fisch, "Nanophotonics for quantum optics using nitrogen-vacancy centers in diamond," Nanotechnology **21**, 274008 (2010).
196. L. Robledo, L. Childress, H. Bernien, B. Hensen, P. F. A. Alkemade, and R. Hanson, "High-fidelity projective read-out of a solid-state spin quantum register," Nature **477**, 574–578 (2011).
197. P. Tamarat, T. Gaebel, J. R. Rabeau, M. Khan, A. D. Greentree, H. Wilson, L. C. L. Hollenberg, S. Prawer, P. Hemmer, F. Jelezko, and J. Wrachtrup, "Stark shift control of single optical centers in diamond," Phys. Rev. Lett. **97**, 083002 (2006).
198. L. C. Bassett, F. J. Heremans, C. G. Yale, B. B. Buckley, and D. D. Awschalom, "Electrical tuning of single nitrogen-vacancy center optical transitions enhanced by photoinduced fields," Phys. Rev. Lett. **107**, 266403 (2011).
199. V. M. Acosta, C. Santori, A. Faraon, Z. Huang, K.-M. C. Fu, A. Stacey, D. A. Simpson, K. Ganesan, S. Tomljenovic-Hanic, A. D. Greentree, S. Prawer, and R. G. Beausoleil, "Dynamic stabilization of the optical resonances of single nitrogen-vacancy centers in diamond," Phys. Rev. Lett. **108**, 206401 (2012).
200. S. Sun, J. L. Zhang, K. A. Fischer, M. J. Burek, C. Dory, K. G. Lagoudakis, Y.-K. Tzeng, M. Radulaski, Y. Kelaita, A. Safavi-Naeini, Z.-X. Shen, N. A. Melosh, S. Chu, M. Lončar, and J. Vučković, "Cavity-enhanced Raman emission from a single color center in a solid," Phys. Rev. Lett. **121**, 083601 (2018).
201. S. Meesala, Y.-I. Sohn, B. Pingault, L. Shao, H. A. Atikian, J. Holzgrafe, M. Gündoğan, C. Stavrakas, A. Sipahigil, C. Chia, R. Evans, M. J. Burek, M. Zhang, L. Wu, J. L. Pacheco, J. Abraham, E. Bielejec, M. D. Lukin, M. Atatüre, and M. Lončar, "Strain engineering of the silicon-vacancy center in diamond," Phys. Rev. B **97**, 205444 (2018).
202. B. Machielse, S. Bogdanovic, S. Meesala, S. Gauthier, M. Burek, G. Joe, M. Chalupnik, Y. Sohn, J. Holzgrafe, R. Evans, C. Chia, H. Atikian, M. Bhaskar, D. Sukachev, L. Shao, S. Maity, M. Lukin, and M. Lončar, "Quantum interference of electromechanically stabilized emitters in nanophotonic devices," Phys. Rev. X **9**, 031022 (2019).
203. M. V. G. Dutt, L. Childress, L. Jiang, E. Togan, J. Maze, F. Jelezko, A. S. Zibrov, P. R. Hemmer, and M. D. Lukin, "Quantum register based on individual electronic and nuclear spin qubits in diamond," Science **316**, 1312–1316 (2007).
204. T. H. Taminiau, J. Cramer, T. van der Sar, V. V. Dobrovitski, and R. Hanson, "Universal control and error correction in multi-qubit spin registers in diamond," Nat. Nanotechnol. **9**, 171–176 (2014).
205. F. Jelezko, T. Gaebel, I. Popa, A. Gruber, and J. Wrachtrup, "Observation of coherent oscillations in a single electron spin," Phys. Rev. Lett. **92**, 076401 (2004).
206. B. C. Rose, G. Thiering, A. M. Tyryshkin, A. M. Edmonds, M. L. Markham, A. Gali, S. A. Lyon, and N. P. de Leon, "Strongly anisotropic spin relaxation in the neutral silicon vacancy center in diamond," Phys. Rev. B **98**, 235140 (2018).
207. Z.-H. Zhang, P. Stevenson, G. Thiering, B. C. Rose, D. Huang, A. M. Edmonds, M. L. Markham, S. A. Lyon, A. Gali, and N. P. de Leon, "Optically detected magnetic resonance in the neutral silicon vacancy center in diamond via bound exciton states," arXiv:2004.12544 (2020).
208. G. Thiering and A. Gali, "*Ab initio* magneto-optical spectrum of group-IV vacancy color centers in diamond," Phys. Rev. X **8**, 021063 (2018).
209. L. J. Rogers, K. D. Jahnke, M. H. Metsch, A. Sipahigil, J. M. Binder, T. Teraji, H. Sumiya, J. Isoya, M. D. Lukin, P. Hemmer, and F. Jelezko, "All-optical initialization, readout, and coherent preparation of single silicon-vacancy spins in diamond," Phys. Rev. Lett. **113**, 263602 (2014).
210. B. Pingault, J. N. Becker, C. H. Schulte, C. Arend, C. Hepp, T. Godde, A. I. Tartakovskii, M. Markham, C. Becher, and M. Atatüre, "All-optical formation of coherent dark states of silicon-vacancy spins in diamond," Phys. Rev. Lett. **113**, 263601 (2014).
211. B. Pingault, D.-D. Jarausch, C. Hepp, L. Klintberg, J. N. Becker, M. Markham, C. Becher, and M. Atatüre, "Coherent control of the silicon-vacancy spin in diamond," Nat. Commun. **8**, 15579 (2017).
212. Y.-I. Sohn, S. Meesala, B. Pingault, H. A. Atikian, J. Holzgrafe, M. Gündoğan, C. Stavrakas, M. J. Stanley, A. Sipahigil, J. Choi, M. Zhang, J. L. Pacheco, J. Abraham, E. Bielejec, M. D. Lukin, M. Atatüre, and M. Lončar, "Controlling the coherence of a diamond spin qubit through its strain environment," Nat. Commun. **9**, 2012 (2018).
213. C. J. Ciccarino, J. Flick, I. B. Harris, M. E. Trusheim, D. R. Englund, and P. Narang, "Strong spin-orbit quenching via the product Jahn-Teller effect in neutral group IV artificial atom qubits in diamond," arXiv:2001.07743 (2020).
214. I. Harris, C. J. Ciccarino, J. Flick, D. R. Englund, and P. Narang, "Group III quantum defects in diamond are stable spin-1 color centers," arXiv:1907.12548 (2019).
215. K. T. Butler, D. W. Davies, H. Cartwright, O. Isayev, and A. Walsh, "Machine learning for molecular and materials science," Nature **559**, 547–555 (2018).
216. J. Schmidt, M. R. G. Marques, S. Botti, and M. A. L. Marques, "Recent advances and applications of machine learning in solid-state materials science," npj Comput. Mater. **5**, 83 (2019).
217. S. Haroche, "A short history of cavity quantum electrodynamics," in *Conference on Coherence and Quantum Optics* (Optical Society of America, 2007).
218. G. Rempe, R. J. Thompson, H. J. Kimble, and R. Lalezari, "Measurement of ultralow losses in an optical interferometer," Opt. Lett. **17**, 363–365 (1992).
219. C. J. Hood, H. J. Kimble, and J. Ye, "Characterization of high-finesse mirrors: loss, phase shifts, and mode structure in an optical cavity," Phys. Rev. A **64**, 033804 (2001).
220. M. H. Bitarafan and R. G. DeCorby, "On-chip high-finesse Fabry–Perot microcavities for optical sensing and quantum information," Sensors **17**, 1748 (2017).
221. P. R. Dolan, G. M. Hughes, F. Grazioso, B. R. Patton, and J. M. Smith, "Femtoliter tunable optical cavity arrays," Opt. Lett. **35**, 3556–3558 (2010).
222. C. Derntl, M. Schneider, J. Schalko, A. Bittner, J. Schmiedmayer, U. Schmid, and M. Trupke, "Arrays of open, independently tunable microcavities," Opt. Express **22**, 22111–22120 (2014).
223. A. Muller, E. B. Flagg, J. R. Lawall, and G. S. Solomon, "Ultrahigh-finesse, low-mode-volume Fabry–Perot microcavity," Opt. Lett. **35**, 2293–2295 (2010).
224. J. Gallego, W. Alt, T. Macha, M. Martinez-Dorantes, D. Pandey, and D. Meschede, "Strong Purcell effect on a neutral atom trapped in an open fiber cavity," Phys. Rev. Lett. **121**, 173603 (2018).
225. M. Steiner, H. M. Meyer, C. Deutsch, J. Reichel, and M. Koehl, "Single ion coupled to an optical fiber cavity," Phys. Rev. Lett. **110**, 043003 (2013).
226. D. Wang, H. Kelkar, D. Martin-Cano, T. Utikal, S. Götzinger, and V. Sandoghdar, "Coherent coupling of a single molecule to a scanning Fabry–Perot microcavity," Phys. Rev. X **7**, 021014 (2017).
227. D. Najer, I. Söllner, P. Sekatski, V. Dolique, M. C. Löbl, D. Riedel, R. Schott, S. Starosielec, S. R. Valentin, A. D. Wieck, N. Sangouard, A. Ludwig, and R. J. Warburton, "A gated quantum dot strongly coupled to an optical microcavity," Nature **575**, 622–627 (2019).
228. B. Casabone, C. Deshmukh, S. Liu, D. Serrano, A. Ferrier, T. Hümmer, P. Goldner, D. Hunger, and H. de Riedmatten, "Dynamic control of Purcell enhanced emission of erbium ions in nanoparticles," arXiv:2001.08532 (2020).
229. N. E. Flowers-Jacobs, S. W. Hoch, J. C. Sankey, A. Kashkanova, A. M. Jayich, C. Deutsch, J. Reichel, and J. G. E. Harris, "Fiber-cavity-based optomechanical device," Appl. Phys. Lett. **101**, 221109 (2012).
230. D. Riedel, I. Sollner, B. J. Shields, S. Starosielec, P. Appel, E. Neu, P. Maletinsky, and R. J. Warburton, "Deterministic enhancement

of coherent photon generation from a nitrogen-vacancy center in ultrapure diamond," Phys. Rev. X **7**, 031040 (2017).
231. S. Hausler, J. Benedikter, K. Bray, B. Regan, A. Dietrich, J. Twamley, I. Aharonovich, D. Hunger, and A. Kubanek, "Diamond photonics platform based on silicon vacancy centers in a single-crystal diamond membrane and a fiber cavity," Phys. Rev. B **99**, 165310 (2019).
232. M. Salz, Y. Herrmann, A. Nadarajah, A. Stahl, M. Hettrich, A. Stacey, S. Prawer, D. Hunger, and F. Schmidt-Kaler, "Cryogenic platform for coupling color centers in diamond membranes to a fiber-based microcavity," Appl. Phys. B **126**, 131 (2020).
233. S. B. van Dam, M. Ruf, and R. Hanson, "Optimal design of diamond-air microcavities for quantum networks using an analytical approach," New J. Phys. **20**, 115004 (2018).
234. L. Greuter, S. Starosielec, D. Najer, A. Ludwig, L. Duempelmann, D. Rohner, and R. J. Warburton, "A small mode volume tunable microcavity: development and characterization," Appl. Phys. Lett. **105**, 121105 (2014).
235. D. Riedel, S. Flågan, P. Maletinsky, and R. J. Warburton, "Cavity-enhanced Raman scattering for in situ alignment and characterization of solid-state microcavities," Phys. Rev. Appl. **13**, 014036 (2020).
236. J. Gallego, S. Ghosh, S. K. Alavi, W. Alt, M. Martinez-Dorantes, D. Meschede, and L. Ratschbacher, "High-finesse fiber Fabry–Perot cavities: stabilization and mode matching analysis," Appl. Phys. B **122**, 47 (2016).
237. I. Friel, S. L. Geoghegan, D. J. Twitchen, and G. A. Scarsbrook, "Development of high quality single crystal diamond for novel laser applications," Proc. SPIE **7838**, 783819 (2010).
238. J. Benedikter, T. Huemmer, M. Mader, B. Schlederer, J. Reichel, T. W. Haensch, and D. Hunger, "Transverse-mode coupling and diffraction loss in tunable Fabry–Perot microcavities," New J. Phys. **17**, 053051 (2015).
239. J. Benedikter, T. Moosmayer, M. Mader, T. Hümmer, and D. Hunger, "Transverse-mode coupling effects in scanning cavity microscopy," New J. Phys. **21**, 103029 (2019).
240. K. M. Nowak, H. J. Baker, and D. R. Hall, "Efficient laser polishing of silica micro-optic components," Appl. Opt. **45**, 162–171 (2006).
241. D. Hunger, C. Deutsch, R. J. Barbour, R. J. Warburton, and J. Reichel, "Laser micro-fabrication of concave, low-roughness features in silica," AIP Adv. **2**, 012119 (2012).
242. T. Ruelle, M. Poggio, and F. Braakman, "Optimized single-shot laser ablation of concave mirror templates on optical fibers," Appl. Opt. **58**, 3784–3789 (2019).
243. D. Najer, M. Renggli, D. Riedel, S. Starosielec, and R. J. Warburton, "Fabrication of mirror templates in silica with micron-sized radii of curvature," Appl. Phys. Lett. **110**, 011101 (2017).
244. A. A. P. Trichet, P. R. Dolan, D. M. Coles, G. M. Hughes, and J. M. Smith, "Topographic control of open-access microcavities at the nanometer scale," Opt. Express **23**, 17205–17216 (2015).
245. G. W. Biedermann, F. M. Benito, K. M. Fortier, D. L. Stick, T. K. Loyd, P. D. D. Schwindt, C. Y. Nakakura, R. L. Jarecki, and M. G. Blain, "Ultrasmooth microfabricated mirrors for quantum information," Appl. Phys. Lett. **97**, 181110 (2010).
246. G. Wachter, S. Kuhn, S. Minniberger, C. Salter, P. Asenbaum, J. Millen, M. Schneider, J. Schalko, U. Schmid, A. Felgner, D. Hüser, M. Arndt, and M. Trupke, "Silicon microcavity arrays with open access and a finesse of half a million," Light Sci. Appl. **8**, 37 (2019).
247. S. Bogdanovic, M. S. Z. Liddy, S. B. van Dam, L. C. Coenen, T. Fink, M. Lončar, and R. Hanson, "Robust nano-fabrication of an integrated platform for spin control in a tunable microcavity," APL Photon. **2**, 126101 (2017).
248. A. H. Piracha, P. Rath, K. Ganesan, S. Kühn, W. H. P. Pernice, and S. Prawer, "Scalable fabrication of integrated nanophotonic circuits on arrays of thin single crystal diamond membrane windows," Nano Lett. **16**, 3341–3347 (2016).
249. P. Ovartchaiyapong, L. M. A. Pascal, B. A. Myers, P. Lauria, and A. C. Bleszynski Jayich, "High quality factor single-crystal diamond mechanical resonators," Appl. Phys. Lett. **101**, 163505 (2012).
250. Y. Tao, J. M. Boss, B. A. Moores, and C. L. Degen, "Single-crystal diamond nanomechanical resonators with quality factors exceeding one million," Nat. Commun. **5**, 3638 (2014).
251. P. Latawiec, V. Venkataraman, M. J. Burek, B. J. M. Hausmann, I. Bulu, and M. Lončar, "On-chip diamond Raman laser," Optica **2**, 924–928 (2015).
252. P. Appel, E. Neu, M. Ganzhorn, A. Barfuss, M. Batzer, M. Gratz, A. Tschöpe, and P. Maletinsky, "Fabrication of all diamond scanning probes for nanoscale magnetometry," Rev. Sci. Instrum. **87**, 063703 (2016).
253. S. Sangtawesin, B. L. Dwyer, S. Srinivasan, J. J. Allred, L. V. Rodgers, K. De Greve, A. Stacey, N. Dontschuk, K. M. O'Donnell, D. Hu, D. A. Evans, C. Jaye, D. A. Fischer, M. L. Markham, D. J. Twitchen, H. Park, M. D. Lukin, and N. P. de Leon, "Origins of diamond surface noise probed by correlating single-spin measurements with surface spectroscopy," Phys. Rev. X **9**, 031052 (2019).
254. D. Riedel, "Engineering of the photonic environment of single nitrogen-vacancy centers in diamond," Ph.D. thesis (University of Basel, 2017).
255. S. Bogdanovic, S. B. van Dam, C. Bonato, L. C. Coenen, A.-M. J. Zwerver, B. Hensen, M. S. Z. Liddy, T. Fink, A. Reiserer, M. Lončar, and R. Hanson, "Design and low-temperature characterization of a tunable microcavity for diamond-based quantum networks," Appl. Phys. Lett. **110**, 171103 (2017).
256. J. F. S. Brachmann, H. Kaupp, T. W. Hänsch, and D. Hunger, "Photothermal effects in ultra-precisely stabilized tunable microcavities," Opt. Express **24**, 21205 (2016).
257. E. Janitz, M. Ruf, Y. Fontana, J. Sankey, and L. Childress, "High mechanical bandwidth fiber-coupled Fabry-Perot cavity," Opt. Express **25**, 20932–20943 (2017).
258. T. W. Hänsch and B. Couillaud, "Laser frequency stabilization by polarization spectroscopy of a reflecting reference cavity," Opt. Commun. **35**, 441–444 (1980).
259. M. Hanks, M. Trupke, J. Schmiedmayer, W. J. Munro, and K. Nemoto, "High-fidelity spin measurement on the nitrogen-vacancy center," New J. Phys. **19**, 103002 (2017).
260. K. Nemoto, M. Trupke, S. J. Devitt, B. Scharfenberger, K. Buczak, J. Schmiedmayer, and W. J. Munro, "Photonic quantum networks formed from NV-centers," Sci. Rep. **6**, 26284 (2016).
261. M. Hanks, N. L. Piparo, M. Trupke, J. Schmiedmayer, W. J. Munro, and K. Nemoto, "A universal quantum module for quantum communication, computation, and metrology," Proc. SPIE **10358**, 103580K (2017).
262. M. Trupke, C. Salter, S. Reisenbauer, R. Vasconcelos, G. Wachter, K. Buczak, A. Angerer, J. Schmiedmayer, F. Aumayr, U. Schmid, P. Walther, W. J. Munro, and K. Nemoto, "Large-scale quantum technology based on luminescent centers in crystals," in *IEEE International Electron Devices Meeting (IEDM)* (2016), pp. 13.7.1–13.7.4.
263. J. D. Joannopoulos, S. G. Johnson, J. N. Winn, and R. D. Meade, *Photonic Crystals: Molding the Flow of Light*, 2nd ed. (Princeton University, 2011).
264. J. T. Robinson, C. Manolatou, L. Chen, and M. Lipson, "Ultrasmall mode volumes in dielectric optical microcavities," Phys. Rev. Lett. **95**, 143901 (2005).
265. S. Hu and S. M. Weiss, "Design of photonic crystal cavities for extreme light concentration," ACS Photon. **3**, 1647–1653 (2016).
266. H. Choi, M. Heuck, and D. Englund, "Self-similar nanocavity design with ultrasmall mode volume for single-photon nonlinearities," Phys. Rev. Lett. **118**, 223605 (2017).
267. X. Qiang, X. Zhou, J. Wang, C. M. Wilkes, T. Loke, S. O'Gara, L. Kling, G. D. Marshall, R. Santagati, T. C. Ralph, J. B. Wang, J. L. O'Brien, M. G. Thompson, and J. C. F. Matthews, "Large-scale silicon quantum photonics implementing arbitrary two-qubit processing," Nat. Photonics **12**, 534–539 (2018).
268. C. Papon, X. Zhou, H. Thyrrestrup, Z. Liu, S. Stobbe, R. Schott, A. D. Wieck, A. Ludwig, P. Lodahl, and L. Midolo, "Nanomechanical single-photon routing," Optica **6**, 524–530 (2019).
269. A. F. Koenderink, A. Alù, and A. Polman, "Nanophotonics: shrinking light-based technology," Science **348**, 516–521 (2015).
270. M. J. Burek, Y. Chu, M. S. Z. Liddy, P. Patel, J. Rochman, S. Meesala, W. Hong, Q. Quan, M. D. Lukin, and M. Lončar, "High quality-factor optical nanocavities in bulk single-crystal diamond," Nat. Commun. **5**, 5718 (2014).
271. I. Aharonovich and E. Neu, "Diamond nanophotonics," Adv. Opt. Mater. **2**, 911–928 (2014).
272. M. Mitchell, D. P. Lake, and P. E. Barclay, "Realizing $Q > 300\,000$ in diamond microdisks for optomechanics via etch optimization," APL Photon. **4**, 016101 (2019).
273. B. Khanaliloo, M. Mitchell, A. C. Hryciw, and P. E. Barclay, "High-Q/V monolithic diamond microdisks fabricated with quasi-isotropic etching," Nano Lett. **15**, 5131–5136 (2015).

274. B. J. M. Hausmann, B. Shields, Q. Quan, P. Maletinsky, M. McCutcheon, J. T. Choy, T. M. Babinec, A. Kubanek, A. Yacoby, M. D. Lukin, and M. Loncar, "Integrated diamond networks for quantum nanophotonics," Nano Lett. **12**, 1578–1582 (2012).
275. C. F. Wang, E. L. Hu, J. Yang, and J. E. Butler, "Fabrication of suspended single crystal diamond devices by electrochemical etch," J. Vac. Sci. Technol. B **25**, 730–733 (2007).
276. I. Bayn, B. Meyler, A. Lahav, J. Salzman, R. Kalish, B. A. Fairchild, S. Prawer, M. Barth, O. Benson, T. Wolf, P. Siyushev, F. Jelezko, and J. Wrachtrup, "Processing of photonic crystal nanocavity for quantum information in diamond," Diam. Relat. Mater. **20**, 937–943 (2011).
277. J. Riedrich-Möller, L. Kipfstuhl, C. Hepp, E. Neu, C. Pauly, F. Mücklich, A. Baur, M. Wandt, S. Wolff, M. Fischer, S. Gsell, M. Schreck, and C. Becher, "One- and two-dimensional photonic crystal microcavities in single crystal diamond," Nat. Nanotechnol. **7**, 69–74 (2012).
278. B. Jalali and S. Fathpour, "Silicon photonics," J. Lightwave Technol. **24**, 4600–4615 (2006).
279. J. E. Butler, R. L. Woodin, L. M. Brown, P. Fallon, A. H. Lettington, and J. W. Steeds, "Thin film diamond growth mechanisms," Philos. Trans. R. Soc. A **342**, 209–224 (1993).
280. X. Jiang and C. P. Klages, "Heteroepitaxial diamond growth on (100) silicon," Diam. Relat. Mater. **2**, 1112–1113 (1993).
281. M. Schreck, H. Roll, and B. Stritzker, "Diamond/Ir/$SrTiO_3$: a material combination for improved heteroepitaxial diamond films," Appl. Phys. Lett. **74**, 650–652 (1999).
282. T. Teraji, "Chemical vapor deposition of homoepitaxial diamond films," Phys. Status Solidi A **203**, 3324–3357 (2006).
283. P. Rath, N. Gruhler, S. Khasminskaya, C. Nebel, C. Wild, and W. H. P. Pernice, "Waferscale nanophotonic circuits made from diamond-on-insulator substrates," Opt. Express **21**, 11031–11036 (2013).
284. G. S. Sandhu and W. K. Chu, "Reactive ion etching of diamond," Appl. Phys. Lett. **55**, 437–438 (1989).
285. M. J. Burek, "Free-standing nanomechanical and nanophotonic structures in single-crystal diamond," Ph.D. thesis (Harvard University, 2016).
286. A. Faraon, C. Santori, Z. Huang, V. Acosta, and R. Beausoleil, "Coupling of nitrogen-vacancy centers to photonic crystal cavities in monocrystalline diamond," Phys. Rev. Lett. **109**, 033604 (2012).
287. N. R. Parikh, J. D. Hunn, E. McGucken, M. L. Swanson, C. W. White, R. A. Rudder, D. P. Malta, J. B. Posthill, and R. J. Markunas, "Single-crystal diamond plate liftoff achieved by ion implantation and subsequent annealing," Appl. Phys. Lett. **61**, 3124–3126 (1992).
288. P. Olivero, S. Rubanov, P. Reichart, B. C. Gibson, S. T. Huntington, J. Rabeau, A. D. Greentree, J. Salzman, D. Moore, D. N. Jamieson, and S. Prawer, "Ion-beam-assisted lift-off technique for three-dimensional micromachining of freestanding single-crystal diamond," Adv. Mater. **17**, 2427–2430 (2005).
289. B. A. Fairchild, P. Olivero, S. Rubanov, A. D. Greentree, F. Waldermann, R. A. Taylor, I. Walmsley, J. M. Smith, S. Huntington, B. C. Gibson, D. N. Jamieson, and S. Prawer, "Fabrication of ultrathin single-crystal diamond membranes," Adv. Mater. **20**, 4793–4798 (2008).
290. N. H. Wan, S. Mouradian, and D. Englund, "Two-dimensional photonic crystal slab nanocavities on bulk single-crystal diamond," Appl. Phys. Lett. **112**, 141102 (2018).
291. I. Bayn, B. Meyler, J. Salzman, and R. Kalish, "Triangular nanobeam photonic cavities in single-crystal diamond," New J. Phys. **13**, 025018 (2011).
292. M. J. Burek, N. P. de Leon, B. J. Shields, B. J. M. Hausmann, Y. Chu, Q. Quan, A. S. Zibrov, H. Park, M. D. Lukin, and M. Lončar, "Free-standing mechanical and photonic nanostructures in single-crystal diamond," Nano Lett. **12**, 6084–6089 (2012).
293. H. A. Atikian, P. Latawiec, M. J. Burek, Y.-I. Sohn, S. Meesala, N. Gravel, A. B. Kouki, and M. Lončar, "Freestanding nanostructures via reactive ion beam angled etching," APL Photon. **2**, 051301 (2017).
294. B. Khanaliloo, H. Jayakumar, A. C. Hryciw, D. P. Lake, H. Kaviani, and P. E. Barclay, "Single-crystal diamond nanobeam waveguide optomechanics," Phys. Rev. X **5**, 041051 (2015).
295. S. Mouradian, N. H. Wan, T. Schröder, and D. Englund, "Rectangular photonic crystal nanobeam cavities in bulk diamond," Appl. Phys. Lett. **111**, 021103 (2017).
296. M. Kiss, T. Graziosi, A. Toros, T. Scharf, C. Santschi, O. J. F. Martin, and N. Quack, "High-quality single crystal diamond diffraction gratings fabricated by crystallographic etching," Opt. Express **27**, 30371–30379 (2019).
297. J. L. Zhang, S. Sun, M. J. Burek, C. Dory, Y.-K. Tzeng, K. A. Fischer, Y. Kelaita, K. G. Lagoudakis, M. Radulaski, Z.-X. Shen, N. A. Melosh, S. Chu, M. Lončar, and J. Vučković, "Strongly cavity-enhanced spontaneous emission from silicon-vacancy centers in diamond," Nano Lett. **18**, 1360–1365 (2018).
298. R. E. Evans, M. K. Bhaskar, D. D. Sukachev, C. T. Nguyen, A. Sipahigil, M. J. Burek, B. Machielse, G. H. Zhang, A. S. Zibrov, E. Bielejec, H. Park, M. Lončar, and M. D. Lukin, "Photon-mediated interactions between quantum emitters in a diamond nanocavity," Science **362**, 662–665 (2018).
299. B. J. M. Hausmann, I. B. Bulu, P. B. Deotare, M. McCutcheon, V. Venkataraman, M. L. Markham, D. J. Twitchen, and M. Lončar, "Integrated high-quality factor optical resonators in diamond," Nano Lett. **13**, 1898–1902 (2013).
300. P. Rath, S. Khasminskaya, C. Nebel, C. Wild, and W. H. P. Pernice, "Grating-assisted coupling to nanophotonic circuits in microcrystalline diamond thin films," Beilstein J. Nanotechnol. **4**, 300–305 (2013).
301. C. Dory, D. Vercruysse, K. Y. Yang, N. V. Sapra, A. E. Rugar, S. Sun, D. M. Lukin, A. Y. Piggott, J. L. Zhang, M. Radulaski, K. G. Lagoudakis, L. Su, and J. Vuckovic, "Inverse-designed diamond photonics," Nat. Commun. **10**, 3309 (2019).
302. T. G. Tiecke, K. P. Nayak, J. D. Thompson, T. Peyronel, N. P. D. Leon, V. Vuletić, and M. D. Lukin, "Efficient fiber-optical interface for nanophotonic devices," Optica **2**, 70–75 (2015).
303. S. Mosor, J. Hendrickson, B. C. Richards, J. Sweet, G. Khitrova, H. M. Gibbs, T. Yoshie, A. Scherer, O. B. Shchekin, and D. G. Deppe, "Scanning a photonic crystal slab nanocavity by condensation of xenon," Appl. Phys. Lett. **87**, 141105 (2005).
304. L. Li, T. Schröder, E. H. Chen, M. Walsh, I. Bayn, J. Goldstein, O. Gaathon, M. E. Trusheim, M. Lu, J. Mower, M. Cotlet, M. L. Markham, D. J. Twitchen, and D. Englund, "Coherent spin control of a nanocavity-enhanced qubit in diamond," Nat. Commun. **6**, 6173 (2015).
305. B. Myers, A. Das, M. Dartiailh, K. Ohno, D. Awschalom, and A. Bleszynski Jayich, "Probing surface noise with depth-calibrated spins in diamond," Phys. Rev. Lett. **113**, 027602 (2014).
306. G. D. Lange, Z. H. Wang, D. Ristè, V. V. Dobrovitski, and R. Hanson, "Universal dynamical decoupling of a single solid-state spin from a spin bath," Science **330**, 60–63 (2010).
307. C. G. Yale, B. B. Buckley, D. J. Christle, G. Burkard, F. J. Heremans, L. C. Bassett, and D. D. Awschalom, "All-optical control of a solid-state spin using coherent dark states," Proc. Natl. Acad. Sci. USA **110**, 7595–7600 (2013).
308. J. N. Becker, B. Pingault, D. Groß, M. Gündoğan, N. Kukharchyk, M. Markham, A. Edmonds, M. Atatüre, P. Bushev, and C. Becher, "All-optical control of the silicon-vacancy spin in diamond at millikelvin temperatures," Phys. Rev. Lett. **120**, 053603 (2018).
309. S. M. Meenehan, J. D. Cohen, S. Gröblacher, J. T. Hill, A. H. Safavi-Naeini, M. Aspelmeyer, and O. Painter, "Silicon optomechanical crystal resonator at millikelvin temperatures," Phys. Rev. A **90**, 011803 (2014).
310. S. Maity, L. Shao, S. Bogdanović, S. Meesala, Y.-I. Sohn, N. Sinclair, B. Pingault, M. Chalupnik, C. Chia, L. Zheng, K. Lai, and M. Lončar, "Coherent acoustic control of a single silicon vacancy spin in diamond," Nat. Commun. **11**, 193 (2020).
311. B. J. M. Hausmann, B. J. Shields, Q. Quan, Y. Chu, N. P. de Leon, R. Evans, M. J. Burek, A. S. Zibrov, M. Markham, D. J. Twitchen, H. Park, M. D. Lukin, and M. LoncÇŽr, "Coupling of NV centers to photonic crystal nanobeams in diamond," Nano Lett. **13**, 5791–5796 (2013).
312. J. Riedrich-Möller, C. Arend, C. Pauly, F. Mücklich, M. Fischer, S. Gsell, M. Schreck, and C. Becher, "Deterministic coupling of a single silicon-vacancy color center to a photonic crystal cavity in diamond," Nano Lett. **14**, 5281–5287 (2014).
313. J. Majer, J. M. Chow, J. M. Gambetta, J. Koch, B. R. Johnson, J. A. Schreier, L. Frunzio, D. I. Schuster, A. A. Houck, A. Wallraff, A. Blais, M. H. Devoret, S. M. Girvin, and R. J. Schoelkopf, "Coupling superconducting qubits via a cavity bus," Nature **449**, 443–447 (2007).
314. J. Borregaard, P. Kómár, E. Kessler, A. Sørensen, and M. Lukin, "Heralded quantum gates with integrated error detection in optical cavities," Phys. Rev. Lett. **114**, 110502 (2015).

315. A. Habib Piracha, K. Ganesan, D. W. M. Lau, A. Stacey, L. P. McGuinness, S. Tomljenovic-Hanic, and S. Prawer, "Scalable fabrication of high-quality, ultra-thin single crystal diamond membrane windows," Nanoscale **8**, 6860–6865 (2016).
316. R. Nelz, J. Görlitz, D. Herrmann, A. Slablab, M. Challier, M. Radtke, M. Fischer, S. Gsell, M. Schreck, C. Becher, and E. Neu, "Toward wafer-scale diamond nano- and quantum technologies," APL Mater. **7**, 011108 (2019).
317. S. L. Mouradian, T. Schröder, C. B. Poitras, L. Li, J. Goldstein, E. H. Chen, M. Walsh, J. Cardenas, M. L. Markham, D. J. Twitchen, M. Lipson, and D. Englund, "Scalable integration of long-lived quantum memories into a photonic circuit," Phys. Rev. X **5**, 031009 (2015).
318. H. A. Atikian, A. Eftekharian, A. Jafari Salim, M. J. Burek, J. T. Choy, A. Hamed Majedi, and M. Lončar, "Superconducting nanowire single photon detector on diamond," Appl. Phys. Lett. **104**, 122602 (2014).
319. P. Rath, O. Kahl, S. Ferrari, F. Sproll, G. Lewes-Malandrakis, D. Brink, K. Ilin, M. Siegel, C. Nebel, and W. Pernice, "Superconducting single-photon detectors integrated with diamond nanophotonic circuits," Light Sci. Appl. **4**, e338 (2015).
320. A. Dréau, A. Tchebotareva, A. E. Mahdaoui, C. Bonato, and R. Hanson, "Quantum frequency conversion of single photons from a nitrogen-vacancy center in diamond to telecommunication wavelengths," Phys. Rev. Appl. **9**, 064031 (2018).
321. N. Maring, D. Lago-Rivera, A. Lenhard, G. Heinze, and H. D. Riedmatten, "Quantum frequency conversion of memory-compatible single photons from 606 nm to the telecom C-band," Optica **5**, 507–513 (2018).
322. A. Tchebotareva, S. L. Hermans, P. C. Humphreys, D. Voigt, P. J. Harmsma, L. K. Cheng, A. L. Verlaan, N. Dijkhuizen, W. de Jong, A. Dréau, and R. Hanson, "Entanglement between a diamond spin qubit and a photonic time-bin qubit at telecom wavelength," Phys. Rev. Lett. **123**, 063601 (2019).
323. A. Faraon, C. Santori, Z. Huang, K.-M. C. Fu, V. M. Acosta, D. Fattal, and R. G. Beausoleil, "Quantum photonic devices in single-crystal diamond," New J. Phys. **15**, 025010 (2013).